P.98

SIMULATION STUDIES FOR SURFACES AND MATERIALS STRENGTH

Semiannual Progress Report

for
Cooperative Agreement NCC2-297

for the period
November 1, 1991 - April 30, 1991

Submitted to

National Aeronautics and Space Administration
Ames Research Center
Moffett Field, CA 94035

Computational Chemistry Branch
Dr. Steve Langhoff, Chief

Thermosciences Division
Dr. Jim Arnold, Chief

Prepared by
Eloret Institute
1178 Maraschino Drive
Sunnyvale, CA 94087
Phone: 408 730-8422 and 415 493-4710
K. Heinemann, President and Grant Administrator
Timur Halicioglu, Principal Investigator

(NASA-CR-190340) SIMULATION STUDIES FOR SURFACES AND MATERIALS STRENGTH Semiannual Progress Report, 1 Nov. 1991 - 30 Apr. 1992 (Eloret Corp.) 98 p

N92-26265

Unclas
G3/76 0091236

During this period investigations were carried out in two areas:

1. Energy- and structure-related properties of small gold clusters deposited on the GaAs(110) surface were investigated in this work using a molecular dynamics procedure. A recently developed potential energy function based on two- and three-body interactions was employed in calculating energies and forces. These calculations produced some consistent results with experiments. Calculations indicate that Au atoms adsorbed on the GaAs(110) surface do not favor the formation of 3D clusters at the very early stages of deposition (i.e, up to Au_5). In all cases, gold atoms were found to prefer sites near Ga atoms. Sites for Au near As atoms are energetically less favorable. Furthermore, the present study suggests that three-body interactions involving triplets of Au and As atoms play an important role in determining sites and binding energies for deposited Au atoms on the GaAs(110) surface. Results and the method of calculation are given in Appendix 1.

2. A comparative study was conducted in this part for six classical many-body potentials developed recently for silicon systems. Extensive static calculations were performed using these potentials on small Si clusters, bulk point defects, elastic constants, polytypes, pressure induced phase transformations and low index plane surfaces. Similarities and differences between six potentials were identified and their transferability as well as their accuracy with respect to experiment and first-principles methods were assessed. In general, all these potentials do a relatively poor job of modeling the energetic of small clusters as well as the various reconstructions of the Si(111) surface. They, however, provide a fair to good description of the properties of bulk diamond cubic silicon, its intrinsic defects, and of the Si(100) surface. Besides the fact that none of them model π-bonding, their inability to be more transferable lies in their inadequate description of the angular forces. Each potential has its strengths and limitations but none appears to be clearly su-

perior to the others and none is totally transferrable, However, despite their shortcomings we feel that some of these potentials will be useful in large scale simulations of materials-related problems. They can give valuable insights into phenomana which are otherwise intractable to investigate either experimentally or via first-principles methods. Details of this investigation are presented in Appendix 2.

APPENDIX 1.

SIMULATION CALCULATIONS FOR GOLD CLUSTERS ON THE GaAs(110) SURFACE

Introduction

Due to its increasing technological importance in recent years, numerous experimental as well as theoretical investigations have been carried out in the area of metal-semicontactor interfaces. Today, structural aspects of such interfaces related to atomic configurations in particular, are highly desired. Simulation calculations are carried out here to analyze some of the energy- and structure-related properties of the Au/GaAs interface at an atomic level. In this study, small clusters of gold with varying number of atoms were deposited on the GaAs(110) surface. Calculations were carried out to determine binding energies of the clusters as well as the energetically most favorable binding sites for deposited gold atoms.

Method of Calculation

A molecular dynamics procedure based on the Nordsieck-Gear algorithm was employed here. Calculations were performed considering a potential function based on two- and three-body interactions. The total energy of interaction of a system of N particles was calculated as:

$$\Phi = \sum_{\substack{i,j \\ i<j}}^{N} u(\vec{r}_i, \vec{r}_j) + \sum_{\substack{i,j,k \\ i<j<k}}^{N} u(\vec{r}_i, \vec{r}_j, \vec{r}_k) \tag{1}$$

where, $u(\vec{r}_i, \vec{r}_j)$ and $u(\vec{r}_i, \vec{r}_j, \vec{r}_k)$, denote the two- and three-body interactions, respectively. The two-body part was represented by the Lennard-Jones pair potential:

$$u(r_{ij}) = \epsilon\left[(\frac{r_o}{r_{ij}})^{12} - 2(\frac{r_o}{r_{ij}})^{6}\right] \tag{2}$$

where, $r_{ij} = |\vec{r}_i - \vec{r}_j|$; r_o represents the equilibrium distance and ϵ denotes the two-body energy at $r_{ij} = r_o$. For the three-body part the Axilrod-Teller triple dipole potential was taken into consideration:

$$u(\vec{r}_i, \vec{r}_j, \vec{r}_k) = \frac{Z(1 + 3Cos\theta_i\, Cos\theta_j\, Cos\theta_k)}{(r_{ij} \cdot r_{ik} \cdot r_{jk})^3} \tag{3}$$

where, $\theta_i, \theta_j, \theta_k$ and r_{ij}, r_{ik}, r_{jk} represent the angles and the sides of the triangle formed by the three particles i, j and k, respectively. The three-body intensity parameter is denoted by Z.

It has been demonstrated that this potential function is able to reproduce several energy- and structure-related properties for GaAs systems [1-4]. In a recent study this same potential function has been parametrized for the Au-Ga-As system and, at the same time, it has been used for determining high energy adsorption sites for a single gold atom deposited on the (110) surface of GaAs [5]. Parameters of the potential function for the Au-Ga-As system are given in Table 1. In the present investigation a similar procedure was employed and calculations were carried out for small clusters of gold atoms (containing up to five Au atoms) deposited on the (110) surface of GaAs. Simulations were performed for the low temperature case (T$\approx$1 K), and a time step of 1.4×10^{-15} sec. was considered throughout this study. Also, periodic boundary conditions were employed in two directions to provide continuity for the exposed surface. The (110) surface was generated, first, as an abrupt termination of a properly oriented GaAs lattice. Next, Au atoms were deposited on this ideal surface and the system was equilibrated under the molecular dynamics code. In general, for varying numbers and positions of gold adatoms deposited on GaAs(110), an average of 8,000 molecular dynamics steps was found to be sufficient for a complete equilibration of the system. In the present work, however, to assure that the system is fully equilibrated, 10,000 time steps were employed. For the very last 2,000 time steps the temperature rescaling was turned off and calculated values, in each case, were collected for averaging. During this period the temperature remained fairly constant indicating that the system was fully relaxed.

Calculations for the (110) surface were carried out employing a GaAs substrate of 60 unit cells in a (4×3×5) arrangement containing a total of 240 atoms. The exposed surface consisted of 12 (4×3) surface cells. A portion of this surface is depicted in Figure 1. In addition to Ga and As atom positions in the top two layers of the substrate, various energetically favorable sites for Au adatoms are also shown. In the

calculations, deposited Au atoms as well as substrate atoms located in the top two layers were permitted to fully relax. The rest of the substrate atoms in the system were held fixed in their lattice sites, but they were permitted to fully interact with the relaxing atoms. Because the calculations in this study were carried out at a low temperature, Au atoms positioned at the surface often remain trapped at the nearest minimum. To eliminate this undesired situation, therefore, calculations for each cluster, were repeated considering several different initial configurations and only those with lowest energies are reported here.

Results and Discussions

Figure 1 shows favorable binding sites for Au atoms of different clusters deposited on the (110) surface of GaAs. For a single Au atom, one of the favorable binding sites is shown by the letter 'a' in Figure 1. The location of this site along with the binding energy value given in Table 2 for a single Au atom, are consistent with our earlier report [5]. In the case of Au_2, the most favorable sites for Au atoms are 'a' and 'b' positions which are identical high energy sites in two neighboring surface cells. In this case the separation between two Au atoms is quite large ($\sim$ 4 Å). Therefore, for a dimer deposited on the (110) surface the Au-Au interaction is expected to be rather weak and this is reflected in the e_b value given in Table 2. For Au_3, sites 'a', 'b' and 'c' were predicted to be most favorable. The deposited cluster, in this case, is an isoceles triangle and the distance between two Au atoms (forming the equal sides of the triangle) is about 2.5 Å. This is slightly shorter than the Au-Au equilibrium distance (see Table 1). Even though pair-wise interactions between gold atoms are expected to be more attractive, the Au atom at site 'c' is situated in close proximity to three As atoms (two are in the top layer and the other is in the second layer) which form Au-Au-As and Au-As-As trimers with acute angles providing strong repulsive three-body forces. This is reflected in the e_b value for Au_3 which is about 0.21 eV/per Au atom weaker in binding energy than the individual gold atom (see Table 2). For Au_4, sites 'a', 'c', 'd' and 'e' were found to be the most favorable

adsorption sites. In this case, while three Au atoms are located near each other, the forth one, which is in site 'e', is somewhat separated. It is equidistant from atoms at 'c' and 'd' with a separation of about 4.7 Å. At that separation no significant Au-Au interactions are expected coming from the Au atom positioned at the site 'e'. Repulsive three-body interactions, however, in this configuration, arising from Au-Au-As and Au-As-As triplets, were reduced. Accordingly, the value of e_b for Au_4 was found to be decreased indicating that the bonding is somewhat stronger in this case. For Au_5, favorable adsorption sites were found to be 'a', 'c', 'd', 'f' and 'g' as indicated in Figure 1. In this case the two Au atoms located at sites 'f' and 'g' are somewhat separated from atoms at 'a', 'c' and 'd'. Like Au_4, in this case also farther atoms (located at sites 'f' and 'g') are not expected to contribute much Au-Au interaction. Similarly, calculations indicate that repulsive three-body interactions (due to triplets involving Au and As atoms) also remained at a low level. Therefore, the value of the binding energy per atom, e_b, for the Au_5 case as shown in Table 2, did not change much when compared with Au_4.

Based on the potential energy parameters given in Table 1, it is expected that an isolated Au-Ga dimer would be less energetic than an isolated Au-As dimer. On the GaAs (110) surface, however, Au adatoms in general, were found to prefer sites closer to Ga atoms. Present calculations clearly indicate that this is because of strong three-body interactions exhibited by trimers involving Au and As atoms. Judged by the values of the three-body parameters given in Table 1, on the other hand, energies coming from trimers involving Au and Ga atoms are expected to be rather small. The three-body part of the potential function, as given in Eq. 3, provides strong repulsive energies, in particular, for Au-Au-As and Au-As-As trimers with acute angles. Accordingly, surface sites for Au near As atoms become energetically less favorable. This outcome is in general qualitative agreement with various reports [6,7] indicating that Au is prefentially bonded to Ga atoms at the surface. Feenstra [6] using an STM technique measured the lateral distance between a Au adatom and a top layer substrate Ga atom as ~1.4 Å. While this value is consistent with the calculated lateral distance of 1.44 Å between the single Au

adatom and its closest Ga neighbor, present calculations predict that this nearest neighbor Ga atom is located in the second layer.

Conclusions

Calculations indicate that Au atoms adsorbed on the GaAs(110) surface do not favor the formation of 3D clusters at the very early stages of deposition (i.e, up to Au_5). In all cases, gold atoms were found to prefer sites near Ga atoms. Furthermore, the present study suggests that three-body interactions involving triplets of Au and As atoms play an important role in determining sites and binding energies for deposited Au atoms on the GaAs(110) surface. Results obtained in this investigation are strictly based on energetics and no entropic aspects were taken into consideration here. Therefore, it is recommended that extreme care should be exercised when comparing these results with experimental findings.

Table 1. Parameters for the Potential Energy Function [2].

	Two-Body Part	
	ϵ (eV)	r_o (Å)
$Au - Au$	0.9760	2.6685
$Ga - Ga$	1.0039	2.4607
$As - As$	1.1641	2.4913
$Au - Ga$	0.8860	2.5540
$Au - As$	1.7500	2.5350
$Ga - As$	1.7379	2.4481

	Three-Body Part
	Z (eV Å^9)
$Au - Au - Au$	2009.0
$Ga - Ga - Ga$	1826.4
$As - As - As$	2151.9
$Au - Au - Ga$	278.75
$Au - Au - As$	6000.0
$Au - Ga - Ga$	1237.7
$Au - As - As$	5600.0
$Au - Ga - As$	3270.0
$Ga - Ga - As$	1900.0
$Ga - As - As$	4600.0

Table 2. Calculated binding energies for varying numbers of gold atoms deposited on the (110) surface of GaAs. The total binding energy is denoted by E_{tot} and e_b represents the average binding energy per Au adatom. (Energies are given in eV). Letters a through g indicate for each cluster favorable positions of deposited Au atoms on the (110) surface as shown in Figure 1.

Number of Gold Atoms	Sites (See Figure 1)	$-E_{tot}$	$-e_b$
1	a	2.69	2.69
2	a,b	5.44	2.72
3	a,b,c	7.44	2.48
4	a,c,d,e	10.40	2.60
5	a,c,d,f,g	12.90	2.58

References

[1] D.K. Choi, T. Takai, S. Erkoc, T. Halicioglu, and W.A. Tiller, J. Crystal Growth, **85**, 9 (1987).

[2] S. Erkoc, T. Halicioglu, and W.A. Tiller, Phys. Stat. Sol. (b) **157**, K23 (1990).

[3] S.V. Ghaisas, Surf. Sci., **223**, 441 (1989).

[4] J.M. Holender and C. Jedrzejek, Surf. Sci., **247**, 222 (1991).

[5] S. Erkoc, T. Halicioglu, and W.A. Tiller, Phys. Stat. Sol. (b) **156**, K105 (1989).

[6] R. M. Feenstra, Phys. Rev. Lett., **63**, 1412 (1989).

[7] G. Allan and M. Lannoo, J. Vac. Sci. Technol., **B 9**, 2135 (1991).

Figure 1. A schematic top view of the (110) surface. Large and small open circles represent relative positions of Ga atoms located in the first and second layers. Large and small solid circles represent relative positions of As atoms in the first and second layers. Large open circles with letters are favorable sites for Au atoms of deposited clusters. A unit surface cell is indicated by dotted lines.

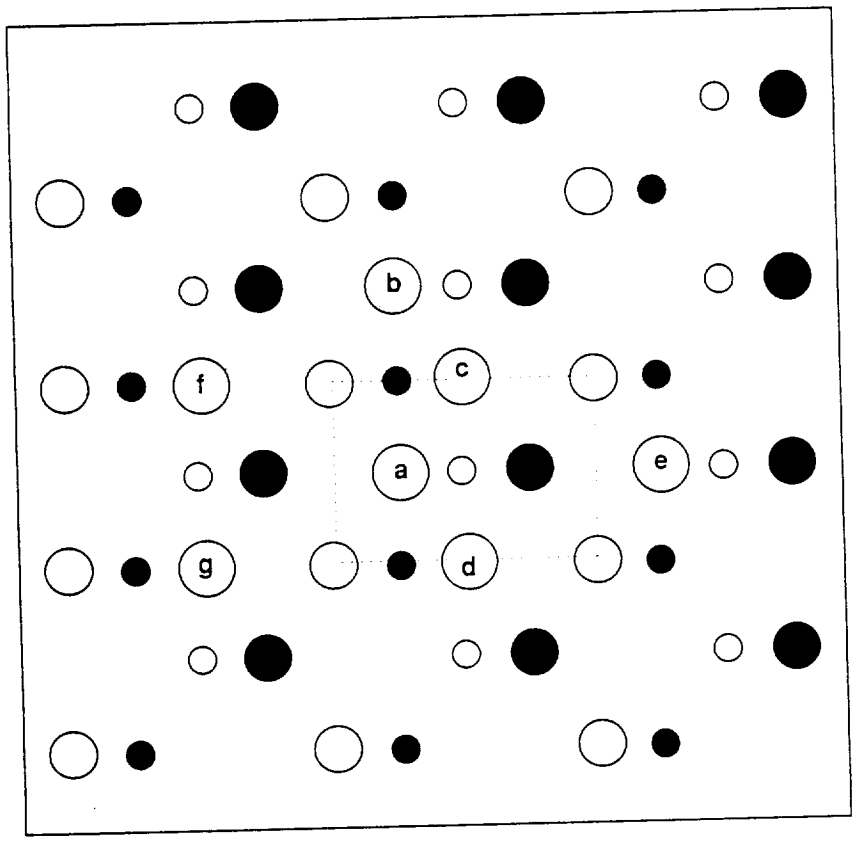

APPENDIX 2.

A COMPARATIVE STUDY OF SILICON EMPIRICAL INTERATOMIC POTENTIALS

1 INTRODUCTION

In recent years, there has been a surge of computer simulations for complex materials science-related phenomena, e.g., molecular dynamics simulations of melting, epitaxy, and crystal growth. In these types of calculations or simulations, it is, of course, desirable to use accurate first-principles quantum-mechanical methods. [1] However, because they require a large computational effort to accurately solve the Schrödinger equation, these methods are currently limited to studies of static properties for systems involving only a few tens of atoms. Nevertheless, progress, although slow, is being made to circumvent these limitations. [2] On the other hand, although they generally lack the accuracy of the former methods, empirical interatomic potentials can handle much larger systems and can be used to study static as well as dynamic properties of such systems.

The theory of interatomic potentials for ionic systems and metals is rather well established as indicated by the remarkable success of some methods, e.g., the shell model [3] and the embedded atom method, [4] to accurately predict a wide range of properties. Unfortunately, the theory for covalent solids is less developed despite the many attempts of the last several years to model such strongly bonded materials.

Not surprisingly, because of its technological importance, silicon has been the prototype material for developing empirical potentials. About sixteen such potentials have appeared in the literature in the last seven years. [5-22] Of course, every new potential is claimed by its originators to be superior, i.e., more accurate and/or more transferrable than its predecessors. While these claims are often valid to some extent, such improvements are almost always achieved by sacrificing other properties. [10-13] Also, very often it is not truly clear what causes the better description. Is it due simply to a more flexible functional form and/or a better fitting strategy [10] or does the new potential really give a better description of covalent bonding? [12] Even the question of the range of interactions in covalent solids is not well understood and very often longer range forces [23,24] are arbitrarily neglected for convenience. Due to the complexity of the structural chemistry of silicon and of the empirical nature of these potentials, the answer to these questions is certainly not an easy task. We attempt here to partly address, albeit indirectly, some of these issues by performing a comparative study of six of the aforementioned potentials. We will not consider here the so-called

valence-force potentials which can only describe small distortions from equilibrium. Stoneham, Torres, Masri, and Schober [25] have performed a comparison of eight such potentials for silicon.

The potentials considered in this study are those of Pearson, Takai, Halicioglu, and Tiller (PTHT), [5] Stillinger and Weber (SW), [6] Biswas and Hamann (BH), [10] Tersoff (T2 and T3), [12,13] and Dodson (DOD). [9] These potentials differ in their degrees of sophistication, functional form, and range of interactions; they thus constitute a good representative sample of existing potentials. Only a few comparative studies of some of these potentials have been performed. In general, these studies involved only a few of the potentials mentioned here and were limited to some specific properties of silicon. Khor and Das Sarma [26] used SW, DOD, and the first Tersoff potential (T1) [8] in a study of Si(100) surface reconstruction. Li, Chen, Allen, and Broughton [27] investigated the energy and vibrational spectrum of the Si(111) 7x7 surface using SW and T2. Halicioglu, Pamuk, and Erkoc [28] studied Si_2 - Si_4 and reviewed the results of some bulk and surface properties obtained with PTHT, SW, T1, and DOD. Bartelt, Williams, Phaneuf, Yang, and Das Sarmas [29] used SW, T1, and T2 to model the orientational stability of silicon surfaces including (100), (111), (112), and (113). Finally, Bolding and Andersen [20] performed an extensive study of Si_2 - Si_{10} and compared the results obtained using their potential with those obtained via BH, SW, and T2. Their comparison for bulk and surface properties was more limited.

Here, these potentials are thoroughly tested in a substantial region of configuration space, including small clusters, bulk, and flat surfaces. A great many results are new and, except for the bulk phonon frequencies, all those results already published by other researchers have been reproduced here for consistency and also because very often, they are incomplete. For instance, the calculations for the bulk monovacancy are more complete here since, in contrast to previous studies, we consider and report all possible configurations.

The calculations for clusters (Si_2 - Si_6) were performed here with and without the cutoff function. Results obtained via PTHT and DOD for Si_5 - Si_6 and via T3 for Si_3 - Si_6 are new. For Si_4, the present work (with PTHT and DOD) is more complete than the study of Halicioglu, Pamuk, and Erkoc. [28] Bolding and Andersen [20] performed calculations on Si_2 - Si_{10} using T3 but did not report any specific result. Moreover, although studies were previously performed using BH, SW, and T2, we identify here some new minima for Si_4 -

Si_6. We considered several bulk point defects: monovacancy and four types of interstitials, tetrahedral, hexagonal, bond-centered, and split or dumbbell. New results are presented for all these defect structures (PTHT and DOD), for the bond-centered interstitial (BH), and for the split interstitial (BH and T2). In addition to the three elastic constants of the cubic diamond structure, we also calculated here the pressure derivative of the bulk modulus, B', and Kleinman's internal strain parameter, ζ. All calculations related to the elastic properties are new for PTHT, BH, and DOD. The results for B' (SW, T2, and T3) and for ζ (SW and T3) are also new. For the bulk polytypes of silicon, we considered, in addition to the cubic diamond phase, all structures for which ab initio data is available. These are hexagonal diamond, BC-8, β-tin, simple hexagonal, the cubic phases, HCP, and the graphitic phase. In contrast to some previous studies, [30] the c/a ratios of the β-tin and all hexagonal phases were optimized. We also calculated the bulk modulus of those structures for which ab initio results are available, e.g., BC-8, β-tin, simple hexagonal, and the graphitic phase. The calculations performed with PTHT (hexagonal diamond, BC-8, and simple hexagonal), BH (graphitic phase), SW (BC-8, β-tin, simple hexagonal, and graphitic phase), DOD (BC-8 and simple hexagonal), T2 (BC-8), and T3 (β-tin and simple hexagonal) are new. The results for the pressure-induced phase transformations are new. Takai [30] reported that cubic diamond transforms under pressure to the β-tin phase but the c/a parameter of this structure was not optimized. Also, Biswas and Hamann [10] reported a transition under pressure from cubic diamond to simple cubic; we found here that this is only the second transition, the first involves a compressed HCP structure. All results for surfaces obtained with T3 are, in general, new. Other new calculations involving surfaces are: (110) (all potentials except SW); (100) 2x1 (PTHT); (100) c 2x2 (BH, DOD, and T2); (100) Pandey defect structure (PTHT, BH, and T2); (111) 2x1 (SW); (111) 2x2 adatom covered structures (all potentials); (111) (2n+1)x(2n+1) DS and DAS structures with n = 1 - 4 (all potentials except for the 7x7 DAS surface with SW and T2). We also present results for the surface stresses of all these surfaces. In general, our results are in agreement with those already published by other researchers; however, there are some discrepancies, in particular with those involving BH.

By a systematic comparison between these potentials, we identify similarities and differences and attempt to find and understand their origins. We also assess the transferability and accuracy of these potentials with respect to experiment

and first-principles methods and discuss their limits and validity in quantitative modelling of materials phenomena. This paper does not, however, address the question of the theoretical justification or basis of interatomic potentials in semiconductors. This question has been dealt with by Carlsson. [31,32] By highlighting the strengths and weaknesses of these potentials and by presenting such a large number of test results in a complete and clear manner, it is hoped that it will help future users to select those potentials best suited for their needs as well as help future researchers desiring to either improve on these potentials or to develop new schemes.

The potentials are described in Sec. 2. The computational procedure is discussed in Sec. 3. Results for small clusters, bulk phases, and flat surfaces are presented and discussed in Secs. 4, 5, and 6, respectively. Section 7 is a review of other potentials not considered in this work. Finally, a general discussion and conclusions are presented in Sec. 8.

2 POTENTIALS

Following Carlsson's classification, [31] PTHT, BH, and SW will be referred to as cluster potentials and the last three as cluster functionals. SW, DOD, T2, and T3 are first-nearest neighbor models (second neighbor interactions are implicitly included in the bond bending term). BH and PTHT include interactions up to the third and seventh shell, respectively. We will sometimes refer to the former and latter group as the short-ranged and longer-ranged potentials, respectively.

In order to have the units of energy and length in eV and Å, respectively (and also for our own convenience), the notation used by the original authors has been modified. It is, of course, straightforward to recover the original notation. Moreover, except for the PTHT and SW potentials, the parameters listed in Table I are, or correspond to, those given in the original references. The original parameters of PTHT and SW give a bulk cohesive energy for diamond silicon of -5.45 and -4.34 eV, respectively. It is convenient for comparison purposes to have a common basis which we choose as the experimental cohesive energy and lattice parameter of diamond silicon (the lattice parameter is predicted almost exactly by all potentials). Thus for PTHT and SW, both of the original two- and three-body energy parameters are multiplied by the same scale factor of 0.85 and 1.07, respectively. The scaling of the energies, in this manner, does not affect the equilibrium structures previously determined. Note

that vibrational frequencies must be multiplied by the square root of these factors.

2.1 Cluster Potentials

The cluster potentials model bonding with classical two- and three-body potentials. The potential energy function gives the structural energy, E, which is written as,

$$E = \frac{1}{2}\sum_{i,j}{}' V_2(r_{ij}) + \sum_{i,j,k}{}' V_3(r_{ij}, r_{ik}, r_{jk})$$

The primes indicate that all summation indices are distinct. Also because $V_3(i,j,k)$ is symmetric with respect to an interchange of i, j, and k, the more restrictive constraint, $k > j > i$, in the triple sum must be used with PTHT. The condition $k > j$ is used with BH and SW because V_3 is symmetric in only j and k. The parameters listed in Table I correspond to these conditions. In general, the two-body potential is given by,

$$V_2(r) = f_c(r)\left(A_1\varphi_1(r) - A_2\varphi_2(r)\right)$$

where f_c is a cutoff function and φ_s is a decaying function of r. The three-body potentials have different forms and will be given separately for each potential.

2.1.1 The PTHT potential

Pearson, Takai, Halicioglu, and Tiller [5] used the Lennard-Jones and Axilrod-Teller potentials for the two- and three-body terms, respectively. The potential is cut abruptly to zero at the cutoff radius, R_c. In our notation, the functions are:

$$\begin{aligned} f_c(r) &= 1 && \text{if } r < R_c \\ &= 0 && \text{otherwise.} \end{aligned}$$

$$\varphi_s(r) = r^{-\lambda_s} \qquad s = 1,2 \qquad (1)$$

$$V_3(r_{ij},r_{ik},r_{jk}) = Z\,\psi(r_{ij})\,\psi(r_{ik})\,\psi(r_{jk})\,g(\theta_i,\theta_j,\theta_k)$$

$$\psi(r) = \frac{f_c(r)}{r^3}$$

$$g(\theta_i,\theta_j,\theta_k) = 1 + 3\cos\theta_i\cos\theta_j\cos\theta_k$$

θ_i is the angle subtended at atom i by atoms j and k; θ_j and θ_k are defined in a similar manner as shown in Fig. 1.

There is, of course, no theoretical justification for using these potentials (in particular the Axilrod-Teller potential) to describe bonding in a covalent material.[5] These particular functional forms were chosen for purely pragmatic reasons and must, therefore, be viewed only as fitting functions. While the PTHT potential is not flexible enough (particularly with respect to the second derivatives), it is appealing because it has only three adjustable parameters (four if the cutoff radius is included; λ_1 and λ_2 are fixed). This fact can be more appreciated when binary or ternary systems are considered.

The parameters were fitted to a minimal database containing the bond lengths of the dimer and trimer and the lattice parameter and cohesive energy of the diamond structure.[30] The parameterization was done using infinite lattice sums ($R_c = \infty$). All results presented in this work correspond to R_c = 7.3 Å which yields results virtually indistinguishable from those obtained using an infinite cutoff radius. $V_2(r)$ is essentially zero at 7.3 Å. Reducing R_c to 5 Å, i.e., including interactions up to third neighbors only, changes the lattice parameter by less than 0.5%, the bulk cohesive energy by 4% and the elastic constants by less than 10%. Similar changes are expected for surfaces, e.g., for the (111) 1x1 surface, the changes are 2%, 3%, and 9% for the first interlayer contraction, the surface energy, and surface stress, respectively. These changes are much larger if the potential is cut below the third shell. Also, the energetics of those surface defects which induce strong atomic distortions, e.g., surface vacancy and some types of steps, are much more sensitive to the cutoff radius.

The PTHT potential has been extensively used to study bulk phase transitions,[33] surface reconstructions,[30,34-37] surface point defect formation and diffusion,[30,34,38] step reconstruction and interaction[35,39] and their effects on two-dimensional nucleation.[39] The same potential has been extended to binary and ternary systems, e.g., GaAs, Si-GaAs, and Al-GaAs.[40-42]

2.1.2 The Biswas-Hamann potential (BH)

This potential is a simpler version of the original BH potential. [7] The three-body potential is separable. Biswas and Hamann [10] used Gaussians for the radial functions and a Fermi-like function for the cutoff function. These functions are:

$$f_c(r) = \left(1 + \exp\left(\frac{r-\sigma}{\mu}\right)\right)^{-1} \qquad \text{if } r < R_c$$

$$= 0 \qquad \text{otherwise.}$$

$$\varphi_s(r) = e^{-\lambda_s r^2} \qquad s = 1,2$$

$$V_3(r_{ij}, r_{ik}, \theta_i) = \sum_{s=1}^{2} Z_s \psi_s(r_{ij}) \psi_s(r_{ik}) g_s(\theta_i)$$

$$\psi_s(r) = e^{-\alpha_s r^2} f_c(r)$$

$$g_s(\theta_i) = (\cos\theta_i - \cos\theta_o)^{s+1}$$

In the original paper, [10] σ was written as R_c suggesting that it is the cutoff radius; In fact, f_c is 0.5 when $r = \sigma$ (for any value of μ) and 0.03 when $r = 5.0$ Å. However, the results do not seem to be sensitive to R_c as long as $R_c \geq \sigma$. For instance, the lattice parameter and cohesive energy of the diamond structure are 5.4126 Å and -4.6267 eV when R_c is equal to σ; they are 5.4318 and -4.6045 at 5.0 Å and at 3.0 Å they are 5.1565 and -4.9748. All the results presented here were obtained with $R_c = 5.0$ Å. $V_2(r)$ is essentially zero at this value. We have not used the separability of the three-body potential. Compared to the original notation, we have $Z_S = 2B_S$. The fitting database included the cohesive energies of a set of bulk phases, the formation energies of self-interstitials, and the surface energy of diamond Si(111) 1x1 and of metallic simple hexagonal and cubic (100) surfaces obtained from an ab initio LAPW calculation. [10] This potential has been used to study microclusters and bulk point defects, [10] amorphous silicon, [43] cluster and atom deposition on Si(111), [44] amorphous and epitaxial film growth on Si(111), [45] and surface reconstruction. [37]

2.1.3 The Stillinger-Weber potential (SW)

The radial function, φ_S, is given by (1). The other functions are:

$$f_c(r) = \exp\left(\frac{\mu}{r - R_c}\right) \qquad \text{if } r < R_c$$

$$= 0 \qquad \text{otherwise.}$$

$$V_3(r_{ij},r_{ik},r_{jk}) = Z\,\psi(r_{ij})\,\psi(r_{ik})\,g(\theta_i)$$

$$\psi(r) = [f_c(r)]^{\alpha}$$

$$g(\theta_i) = (\cos\theta_i - \cos\theta_o)^2$$

Compared to the original notation,[6] we have $A_1 = \varepsilon AB\sigma^p$, $A_2 = \varepsilon A\sigma^q$, $Z = \varepsilon\lambda$, $R_c = a\sigma$, and $\mu = \sigma$. Note that, besides acting as a cutoff function, f_c defines the attractive branch of V_2 (since $\lambda_2 = 0$) and the radial functions of V_3; therefore, the results are very sensitive to variations in R_c. Stillinger and Weber fitted the parameters to the lattice constant and cohesive energy of the diamond structure with the added constraint that the melting point and the structure of liquid silicon be well described. SW is by far the most widely used potential. It has been used to study clusters,[46,47] lattice dynamics,[27,48,49] bulk point defects,[50] the liquid[6,51] and amorphous[52-55] states, surface diffusion[56,57] and reconstructions,[26,27,29,37,58,59] Si(100) stepped surfaces,[60] the liquid-vapor[61] and crystal-melt interfaces,[51,62] pulsed melting of surfaces,[63] epitaxial growth from the vapor,[64-66] liquid-phase epitaxy,[67-69] and growth of amorphous films via atom deposition.[70] This potential has been extended to Ge,[61,71] sulfur,[72] fluorine,[73] and the Si-F system.[74]

2.2 Cluster Functionals

All the cluster functionals considered here are of the Tersoff type. In this scheme, bonding is modeled with pairwise interactions but with the attractive term depending on the local environment which effectively includes many-body interactions.[8,12] The structural energy has the form,

$$E = \frac{1}{2}\sum_{i,j}{}' f_c(r_{ij})\left(A_1\,\varphi_1(r_{ij}) - A_2\,\varphi_2(r_{ij})\,p(\zeta_{ij})\right) \qquad (2)$$

where p is a measure of the bond order and is a function of the effective coordination number, ζ_{ij}, given by,

$$\zeta_{ij} = \sum_{k\neq i,j} V_3(r_{ij}, r_{ik}, \theta_i)$$

$$V_3(r_{ij}, r_{ik}, \theta_i) = \psi(r_{ij}, r_{ik})\,g(\theta_i)$$

Note that, in general, $p(\zeta_{ij}) \neq p(\zeta_{ji})$. The two-body energy can be extracted from E by rewriting (2) as

$$E = \frac{1}{2}\sum_{i,j}{}' V_2(r_{ij}) + \frac{1}{2}\sum_{i,j}{}' A_2\,\varphi_2(r_{ij}) f_c(r_{ij})\left(1 - p(\zeta_{ij})\right) \qquad (3)$$

If $[1 - p(\zeta_{ij})]$ is replaced with a Taylor expansion about some reference it can be seen how this scheme effectively includes many-body interactions.[75] We will refer to the second term in (3) as the three-body energy.

Brenner[76] showed that the Tersoff formalism is similar to the embedded atom method.[4] The two expressions for the structural energy can be made identical with the proper choice of functional forms and parameters.

2.2.1 The Dodson (DOD) potential

This potential is a simple modification of the first Tersoff potential.[8] The functions are:

$$f_c(r) = \frac{1}{2}\left(1 - \cos\left(\frac{\pi(r - R_c)}{\mu}\right)\right) \quad \text{if} \quad R_c - \mu < r < R_c \qquad (4)$$

$$= 1 \quad \text{if} \quad r \leq R_c - \mu$$

$$= 0 \quad \text{otherwise.}$$

$$\varphi_s(r) = e^{-\lambda_s \cdot r} \qquad s = 1,2 \qquad (5)$$

$$p(\zeta_{ij}) = \exp[-\zeta_{ij}^{n}]$$

$$\psi(r_{ij}, r_{ik}) = \left(\frac{\varphi_2(r_{ik}) f_c(r_{ik})}{\varphi_2(r_{ij}) f_c(r_{ij})} \right)^{\alpha}$$

$$g(\theta_i) = \frac{\beta}{\eta + e^{-\delta \cos\theta_i}}$$

To determine the parameters, Dodson used the lattice parameter and cohesive energy of the diamond cubic, simple cubic, BCC, FCC, and HCP structures, the bond length and energy of the dimer, and the bulk modulus of the diamond structure. To our knowledge, this potential is perhaps the least tested compared to the others. It has been used to study low-energy beam deposition of silicon [77] and surface reconstruction. [9,26,37]

2.2.2 The Tersoff potentials (T2 and T3)

T2 and T3 correspond to two different parameterizations of the same potential. f_c and φ_s are given by (4-5), respectively. The other functions are:

$$p(\zeta_{ij}) = \left(1 + \zeta_{ij}^{n}\right)^{\frac{1}{2n}}$$

$$\psi(r_{ij}, r_{ik}) = f_c(r_{ik}).\exp[\alpha^3.(r_{ij} - r_{ik})^3]$$

$$g(\theta_i) = \beta + \frac{\eta^2}{\delta^2} - \frac{\eta^2}{\delta^2 + (\cos\theta_i - \cos\theta_o)^2}$$

The potential parameters were determined by fitting to a database containing the cohesive energy, lattice parameter, and bulk modulus of the diamond structure, and the cohesive energy of bulk polytypes of silicon. [12,13] For T3, an additional constraint was added in order to reproduce the three elastic constants to within 20%. [13] T2 and T3 were used to study microclusters, [20] lattice

dynamics, [12,13,27] bulk point defects, [12,13,78] the liquid [12,13] and amorphous [13,54] states, surface reconstructions, [12,13,27,29,37] and low-energy beam deposition on Si(100) 2x1. [79] This potential was also extended to carbon [80] and to the systems Si-C and Si-Ge. [81,82]

2.3 Discussion

The two-body functions $V_2(r)$ are plotted in Fig. 2. The open circles correspond to an accurate ab initio calculation (based on MRCI) of the energy of the ground-state of Si_2. [83] The T2 and T3 curves are very similar for $r \leq 2.7$ Å. The attractive branches of the BH and SW curves are also similar over the range $2.4 < r < 3.0$ Å. While the shapes of these curves are different, in general, they all have about the same depth with the exception of DOD which is much stronger. The PTHT curve is the steepest with the largest curvature at the equilibrium bond length; this is reflected in the large values of the vibrational frequency of the dimer and the bulk elastic constants. Note the small bump on the curves of the cluster functionals; this is due to the abrupt cutoff function.

The angular dependence, $g(\theta)$, of the three-body potentials is shown in Fig. 3. The PTHT function is very different from the others; it is the only function which is negative for $\theta \geq 117^o$ resulting (in a few cases) in negative three-body energies for configurations with large bond angles. The DOD curve is a monotonic decreasing function of θ with a minimum at 180^o like the PTHT curve. The other curves have the same shape with a minimum at $\theta = \theta_o$. The T2 curve has a very shallow minimum at $\theta = 90^o$ and is symmetric with respect to that angle. For BH, since α_1 and α_2 are almost equal, $g_1(\theta)(1 + (Z_2/Z_1)g_2(\theta))$ is plotted to show the effect of the $\cos^3\theta$ term which is negligible as shown in Fig. 3. A better comparison of the three-body potentials is provided in Fig. 4 which shows the variations of the three-body energy with angle θ for a triplet of atoms i, j, and k (Fig. 1) with $r_{ij} = r_{ik} = 2.351$ Å (the equilibrium bond length of the diamond phase) and $\theta_i = \theta$. The three-body energy for the cluster functionals is defined as the second term of (3). What is actually plotted in Fig. 4 is the contribution of atom i to the total three-body energy of the triplet. There is no curve for T2 because this energy is essentially zero (on the scale of the plot) for the apex atom in an isoceles triangle; the total three-body energy does not, however, vanish (for $\theta \leq 40^o$) because of the contribution of atoms j and k. One immediate consequence of this is that T2 will favor triplet configurations leading

to an equilateral triangle thus making the total energy almost completely controlled by the two-body potential. PTHT is the most repulsive for small angles less than about 45°, and SW and DOD are stronger than the other potentials for $\theta > 135^{o}$ and $50^{o} \leq \theta \leq 140^{o}$, respectively. One very important result to be discussed later is that all these potentials handle rather well small angular distortions around the tetrahedral angle and, to a lesser extent, those leading to angles somewhat larger than 109°, but with the exception of T2, they completely fail when dealing with small angles ($\leq 80^{o}$). This is fully reflected in the curves of Fig. 4. Finally, the large variations displayed by these functions makes a comparison between the potentials very difficult, indeed.

3 COMPUTATIONAL PROCEDURE

Unless indicated otherwise, all results presented here are static, i.e., T = 0 K. In the static limit, we use the so-called potential approximation where we only deal with the mechanical equivalent of the true thermodynamic properties. [84] The total energy was minimized using a conjugate gradient technique. The minimization is stopped when the force on each atom is at most 0.001 eV/Å (typically 10^{-4} eV/Å). Note that, in general, energies converge more rapidly than stresses. For surface calculations, we used fixed atoms to simulate a rigid underlying substrate and used enough moving layers to minimize the interaction between the exposed surface and the moving-fixed interface.

The surface energy per unit area, γ, is defined as,

$$\gamma = \frac{1}{A}\left(E - NE_c\right) \tag{6}$$

where E is the total energy for the simulation of N atoms with bulk cohesive energy E_c and A is the area of the exposed surface.

The total stress $\tau_{\alpha\beta}$ is given by

$$\tau_{\alpha\beta} = \frac{1}{V}\frac{\partial E}{\partial \varepsilon_{\alpha\beta}}$$

where V is the volume of the system, α and β represent any two of the cartesian coordinates and $\varepsilon_{\alpha\beta}$ is the Lagrangian strain tensor. Since the total potential energy and the stresses are given as a sum of contributions of each

atom in the system, it is natural to define an atomic energy, $e(i)$, and stress, $\chi_{\alpha\beta}(i)$, such that

$$E = \sum_i e(i) \text{ and } \tau_{\alpha\beta} = \frac{1}{V}\sum_i \chi_{\alpha\beta}(i)$$

While the definition of the atomic energy and stresses appears to be arbitrary, the availability of the energy and stress distributions can be very helpful in analyzing complex defect structures. [34,82] Also, they are helpful in assessing any finite-size effect which can be present in the calculation. For example, well away from a defect, e.g., at a surface, the atoms must be representative of the bulk environment; this can be readily checked by looking at these distributions.

A two-dimensional surface-stress tensor, $\sigma_{\alpha\beta}$, can also be defined to further characterize the surface, [85,86]

$$\sigma_{\alpha\beta} = \frac{1}{A}\frac{\partial(A\gamma)}{\partial\varepsilon_{\alpha\beta}} = \gamma\delta_{\alpha\beta} + \frac{\partial\gamma}{\partial\varepsilon_{\alpha\beta}} \qquad (7)$$

where $\delta_{\alpha\beta}$ is the Kronecker delta. For a liquid, the strain derivative in (7) vanishes, and the surface stress, called surface tension, is numerically equal to the surface free energy. For a solid surface, $\partial\gamma/\partial\varepsilon_{\alpha\beta}$ can be positive or negative and can thus lead to a tensile or compressive surface stress. Also, as shown for the (100), (110), and (111) 2x1 surfaces, $\sigma_{\alpha\beta}$ is not necessarily isotropic.

Unless indicated otherwise, all surface energies and stresses will be given in eV/1x1 cell (for simplicity, we will sometimes drop the per 1x1 cell). To obtain γ and $\sigma_{\alpha\beta}$ in eV/Å^2, divide by the area of the 1x1 primitive surface cell. Also, surface energy will refer to the value calculated from (6); the relative energy of a relaxed or reconstructed surface is, in general, its surface energy relative to that of the ideal 1x1 surface.

For point defects, we calculated defect energies both at constant volume and constant zero pressure. For both cases, the reference is the perfect diamond lattice (pressure, P = 0; atomic volume, $\Omega = \Omega_e$) so that the formation energy, E_f is given by,

$$E_f = E - (N \pm 1)\, E_c$$

where E is the total energy for the simulation of (N ± 1) atoms, +1 for a single interstitial and -1 for a monovacancy. We used a large cell containing (980 ± 1) atoms and the cartesian coordinate system was taken as $\hat{x} = [1\bar{1}0]$, $\hat{y} = [00\bar{1}]$, and $\hat{z} = [110]$. Periodic boundary conditions are applied in all three directions in order to simulate a bulk environment. For the constant volume calculation, the cell with a defect has to be compressed (vacancy) or expanded (interstitial) to bring the atomic volume to the equilibrium value, Ω_e. This is done by scaling the lattice parameter by the factor $(1 \pm 1/N)^{1/3}$. For N = 980, the change in lattice parameter is only ± 0.03% but it is ± 0.5% for N = 64. To simulate a constant pressure one would normally use molecular-dynamics or Monte Carlo methods. But these methods are much more time-consuming than a static method. If one is only interested in studying pressure effects at zero temperature on equilibrium structures, it is desirable to devise a static method where the volume is a variable. We have implemented the conventional method used in isobaric Monte Carlo simulation [87] into our static program code.

In the "constant volume" static method, the objective function is the total energy $E\{\mathbf{r}\}$ and the variables are the 3N atomic coordinates $\{\mathbf{r}\}$ in the system of N atoms. The volume, V, of the computational cell is held fixed. In the "constant pressure" version, the enthalpy $H\{\boldsymbol{\rho},V\} = E\{\boldsymbol{\rho},V\} + P_{ex}V$ is minimized. There are now (3N + 1) variables which are V and the 3N dimensionless atomic coordinates, $\{\boldsymbol{\rho} = V^{-1/3}\mathbf{r}\}$. The externally applied pressure, P_{ex}, is set to zero in this work. Note that, like the atomic coordinates, the periodic boundary vectors must be scaled by $V^{-1/3}$ at each iteration step. In practice, we found it necessary to constrain the volume to vary within a prescribed range.

Because very often experimental data are lacking, people involved in atomistic computer simulation rely heavily on results obtained from first-principles calculations, not only for comparison purposes but also for use as input for the parameterization of the interatomic potential. In this work, only the properties of Si_2 and those of the perfect diamond lattice are directly compared to experiment. Other bulk and surface properties are compared to results obtained from ab initio calculations using mostly the self consistent pseudopotential method within the local density functional theory (simply abbreviated DFT from now on). Results for Si_3 - Si_6 are compared with those obtained from an ab initio molecular orbital calculation. [88]

Very often the ab-initio data are obtained from different sources, i.e., different techniques or calculations performed with different input calculational parameters. While the DFT method is certainly one of the most accurate theoretical tools for the calculation of the ground-state properties of solids, [1,89] it is important to keep in mind such differences in the data when making comparisons. Furthermore, for the parameterization of the interatomic potential, it is critical to use consistent and compatible data especially when used in conjunction with some experimental data, which is often the case. While several input calculational parameters can affect the result of the calculation (care is generally taken to minimize the effect of most of them) , the plane-wave cutoff energy, E_{pw}, is the limiting factor. Structural parameters, e.g., the lattice parameters, are weakly dependent on E_{pw}, but energies converge more slowly below about 10 Ry. [89-92] Typically, E_{pw} is about 6 Ry. The effect of E_{pw} can be appreciated by considering the calculation of the energies of adatom-covered Si(111) surfaces. Northrup [93] performed a calculation at 6 Ry and he successfully determined that the T_4 adsorption site is energetically favored over the H_3 site (both sites have three-fold symmetry but the T_4 adatom has a second-layer atom directly below in contrast to the H_3 adatom which does not). He also found that the $\sqrt{3}x\sqrt{3}$ structure was more stable than the 2x2 structure. In fact, the opposite was found to be true by Meade and Vanderbilt who performed a more accurate calculation at 12 Ry. [91] Other examples are provided by the formation energies of bulk point defects in silicon for which extensive calculations lead to uncertainties of up to 2 eV [21,32,94-96] and by the energy of buckled and symmetric dimers on the Si(100) surface for which seemingly similar calculations lead to opposite results (see Sec. 6).

4 CLUSTERS

The only accurate experimental data for silicon clusters are the bond length, bond energy, and vibrational frequency of Si_2 [97] and the binding energy of Si_3. [88] No experimental data on the structures of Si_n ($n \geq 3$) is available. However, accurate ab initio calculations have been performed on microclusters. [88,98] Raghavachari (KR) performed an ab initio molecular-orbital calculation and considered several configurations and electronic states for each Si_n cluster (n = 2 - 6) in order to determine the ground-state structures. [88] The ground-state structures were found to be somewhat compact with an average bond length of

about 2.28 Å (shorter than the equilibrium bond length of the diamond structure) and bond angles in the range 60^{o} - 90^{o}. These structures are significantly different from the configurations derived from microcrystal fragments. These latter lie much higher in energy than the former. The lowest-energy structures for Si_3 - Si_6 are the isoceles triangle, rhombus, trigonal bipyramid, and edge-capped trigonal bipyramid, respectively. Each cluster can be formed from the previous one by attaching an extra atom at an edge- or face-capped site. These Si_n structures are three-dimensional in nature for $n \geq 5$. At the level of theory considered and based on the experimental data of Si_2 and Si_3, KR estimated that only about 80 % of the binding energy of these clusters is recovered. He, thus, scaled the binding energy of all the clusters by the same factor of 1.2. The energies given in Tables II-III are the scaled values.

Several studies on small silicon clusters were performed using some of the potentials considered here. Halicioglu, Pamok, and Erkoc [28] used the PTHT, SW, and DOD potentials for a limited study on Si_2 - Si_4. Biswas and Hamann [10] used their potential along with a combination of steepest descents and simulated annealing techniques to determine the low-energy structures for Si_n clusters (n = 3-6, 10, 32). A molecular dynamics simulation of Si_n clusters (n = 3-17, 32) was performed by Blaisten-Baroja and Levesque using the SW potential. [46] Both neutral and positively charged clusters were examined. Feuston, Kalia, and Vashista [47] also used the SW potential to study the fragmentation of Si_n clusters (n = 2-14) with a molecular dynamics technique. Bolding and Andersen [20] performed a calculation on Si_2 - Si_{10} using BH, SW, T2, and their own potential.

We have performed our own calculations on Si_2 - Si_6 using all six potentials along with a static method. For each potential, except SW, calculations were carried out with and without the cutoff function. Because simple minimization energy techniques are not adequate for finding global minima, we have considered many configurations for each cluster; this includes all geometries considered in previous studies as well as several other structures such as a planar C_{2V} form for Si_5 (edge-capped rhombus) and a C_{5V} form for Si_6 (pentagonal pyramid) as illustrated in Fig. 5. Moreover, many asymmetric structures derived from each of these configurations were optimized. Our results of the calculations *with the cutoff function* are summarized in Tables II-III. Since the energy of atoms infinitely separated is taken as zero, the binding energy, E_B, is the absolute value of the total potential energy as given in Sec. 2.

4.1 Si_2 and Si_3

The equilibrium bond length, r_e, binding energy, D_e, and vibrational frequency, ω_0 of the Si_2 dimer, as obtained from the six potentials are shown in Table II. Most potentials used r_e in the fitting database; it is, therefore, well reproduced by most of them. The largest discrepancy of 5% in r_e occurs with SW. D_e is less well described with a discrepancy ranging from 12% for DOD to -29% for SW. The best description of ω_0 is obtained with DOD; PTHT overestimates it by 50% and the other potentials underestimate it by about 10%.

The ab initio calculations predict that the lowest-energy configuration for Si_3 is an isoceles triangle with an apex bond angle of 77.8° and bond length of 2.165 Å which indicates strong multiple bonding character. [88] It was also shown that the linear structure is only a saddle point on the potential energy surface of Si_3 and that there is also a low-lying state which lies only a few kcal/mol higher in energy; its structure is an equilateral triangle with bond length of 2.263 Å. None of the potentials predicts the correct ground-state structure of Si_3 (see Table II). As expected from Fig. 4, PTHT, T3, and DOD predict a trimer with bond angle of 180°, 126.75°, and 180°, respectively, i.e., the angle at which the three-body energy is a minimum. These three potentials correctly predict the second minimum; they, however, overestimate the bond length. Not surprisingly, as noted in the previous section, T2 predicts an equilateral triangle as the ground-state structure of Si_3. SW and BH were expected to predict an isoceles triangle with a bond angle equal to the tetrahedral angle as the lowest-energy structure which turned out to be an equilateral triangle. BH like T2, does not, however, predict a second minimum. With T2, the bond length and binding energy of Si_3 are constant at 2.31 Å and 5.25 eV for angles larger than 88°. The calculation performed without the cutoff function shows that, for this potential, there is, in addition to the same global minimum, a shallow local minimum corresponding to a linear structure with E_B = 5.2463 eV and a bond length of 2.31 Å (the maximum between these two minima occurs at 120° with E_B = 5.2419 eV).

4.2 Si_4, Si_5, and Si_6

The first three lowest-energy structures for Si_4 - Si_6 are presented in Table III. Some of the structures are illustrated in Fig. 5. The hexagonal chair and the chain are crystal fragments when θ = 109.5°. In the corner-capped triangle, r_{34} is slightly different from r_{13}. The rhombus in the corner- and edge-capped

rhombus is somewhat distorted. For both the trigonal bipyramid and square pyramid, there are two different geometrical arrangements, a flattened and an elongated form. $r_{15} < r_{12}$ in the flat square pyramid and $r_{15} > r_{12}$ in its elongated form; atoms 1, 2, and 3 are bonded to each other in the elongated trigonal bipyramid while they are not in the corresponding flattened form. The wedge is a symmetrical stacking of two equilateral triangles. The orthorhombic bipyramid can be viewed as two edge-sharing distorted tetrahedrons. With PTHT, atoms 1 and 2 are bonded to each other in the asymmetric structure. For the linear structures, the numbering of atoms is from one end to the other as in Ref. 88.

Let us first discuss the ground-state structures. Only PTHT correctly describes the ground-state structure of Si_4, i.e., the rhombus. This structure is predicted to be a local minimum on the potential energy surface by DOD and T2. With BH, SW, and T3, it is not a minimum. For Si_5, the quantum ground-state structure, e.g., the flat trigonal bipyramid, is a local minimum with all potentials (E_B = 10.78 eV with PTHT and 12.03 eV with DOD). The edge-capped trigonal bipyramid, which is the global minimum on the quantum potential energy surface is only a local minimum on the surface generated with PTHT (E_B = 14.18 eV), BH (15.26), SW (14.95), DOD (14.89), T2 (23.08), and T3 (13.13). For the first three potentials, the structural parameters of the optimized structures are very different from those of the quantum structure.

For a potential to be useful in studies of clusters, it should, as pointed out by Bolding and Andersen, [20] give at least a fair representation of the entire potential energy surface. That is, it should not only fairly descibe the energies and structures of global and local minima but also, and perhaps more importantly, not predict spurious minima (minima which do not exist on the quantum potential energy surface). In addition to the global minima, there are three, three, and one known local minima on the ab initio potential energy surface for Si_4, Si_5, and Si_6, respectively. Not listed in Table III are the pyramid (E_B = 9.14 eV) for Si_4, and the pentagon (E_B = 12.10 eV, r = 2.39 Å) for Si_5. KR also reported that, for Si_5, the linear structure and the tetrahedral crystal fragment lie higher in energy than all the other structures and that the former has a larger E_B than the latter. [88] It is not known whether these two structures are minima.

For Si_4, all potentials predict that the tetrahedron is a minimum while the D_{2d} structure is not. The pyramid is predicted to be a local minimum only by SW; however, its apex angle is 109.5° (a crystal fragment) compared to the

value of 78° for the quantum structure. This structure is degenerate in energy with the chain (another crystal fragment). For Si_5, structures that are predicted to be minima are: the elongated trigonal bipyramid by PTHT (E_B = 10.75 eV), T2, and T3 (9.83 eV); the flat square pyramid by T2; and the pentagon by all potentials (for T2, E_B = 13.12 eV, r = 2.31 Å). For Si_6, only BH and SW predict that the hexagonal chair is a local minimum; however, the bond angle is 107.2° and 109.5°, respectively. The value for the optimized quantum structure is 93.6°.

We now consider the spurious minima. KR determined that the following are not minima on the quantum potential energy surface: for Si_4, the corner-capped triangle (E_B = 10.63 eV), the square (10.61 eV; r = 2.32 Å), and the linear structure (8.75 eV); for Si_5, the elongated square pyramid (16.16 eV; r_{12} = 2.30 Å, r_{15} = 2.50 Å); for Si_6, the face-capped trigonal bipyramid (21.87 eV) and the tetragonal bipyramid (21.48 eV). The following structures are thus spurious minima: the square, the corner-capped triangle, and the linear structure (all potentials); the elongated square pyramid (all potentials except T2); face-capped trigonal bipyramid (DOD, T2, and T3); the tetragonal bipyramid (T3). Finally, we should mention that, with all six potentials, we have found many more local minima (about 15 overall for each potential) which, in general, are close in energy.

PTHT and DOD favor planar structures. In fact, PTHT and DOD give rather similar descriptions of the structures of the small Si_n clusters. This is consistent with the similar monotonic angular variations of the three-body energy for relatively larger angles. The most similar potentials are BH and SW. Both predict the same ground-state structure for each cluster. BH gives slightly larger binding energies and smaller bond lengths than SW. T3 is also close to BH and SW. It predicts the same ground-state structures (with similar bond lengths and binding energies) for Si_4 and Si_5. There are more similarities between T3, BH, and SW if all minima for Si_4, Si_5, and Si_6 are considered. That BH and SW and, to lesser extent, T3 are similar can also be traced back to the behavior of the corresponding three-body potentials as shown in Fig. 4. Note the tendency for T3 to also favor planar structures. As expected from our earlier discussion, T2 favors structures which lead to triplets forming an equilateral triangle or close to it. For example, for Si_4, the tetrahedron and rhombus are actually 4 and 2 edge-sharing equilateral triangles, respectively. All three minimum energy structures and also the trimer structure have the same bond length of 2.31 Å, i.e., the equilibrium bond length of the dimer. It is this discrimination in favor of

structures having equilateral triangles as their building blocks which leads to three-dimensional configurations in agreement with the ab initio calculations. In fact, T2 is the potential that provides the fairest overall agreement with the ab initio calculations.

In order to compare the cluster binding energies, a plot of the binding energy per atom versus the number of atoms in the cluster is shown in Fig. 6. The curve labeled KR corresponds to the scaled energies of the ab initio calculations. The similarity noted above for BH, SW, and T3 is also apparent in the binding energy. The PTHT curve is very similar to that of these potentials. The DOD potential, which showed similarities with PTHT for the structures of the Si_n clusters, leads to larger binding energies than PTHT because its two-body potential is stronger. Compared to the scaled ab initio results, PTHT, BH, SW, DOD and T3 generally underestimate the binding energy of the Si_n clusters while T2 overestimates it. Note that, for T2, the energy per atom is increasing with a relatively large slope and it is already 4.42 eV for n=6, i.e., very close to the bulk cohesive energy. This is a direct consequence of the fact that the bond bending forces are very small; thus T2 favors close packed structures because the total energy is almost totally controlled by the two-body potential. A best fit with the KR curve can be obtained for the binding energies by using a scaling factor of 1.43, 1.40, 1.47, 1.15, 0.85, and 1.39 for PTHT, BH, SW, DOD, T2, and T3, respectively. However, this will also change the bulk and surface energies and it will not change the fact that the equilibrium configurations are, in general, in disagreement with the ab initio results. To compare the relative stability of these clusters, and thus look at the possibility of magic numbers, one needs to perform a calculation of the fragmentation energy, E_{fr}. This is the smallest energy involved in the dissociation of Si_n into $Si_{n-m} + Si_m$. An accurate determination of E_{fr} involves the investigation of all possible fragmentation channels. KR determined that E_{fr} corresponds to the process $Si_n \rightarrow Si_{n-1} + Si$ and confirmed the presence of the magic numbers 4 and 6. [88] Using SW, Feuston, Kalia, and Vashista [47] also found the same fragmentation process for Si_n (n = 2 - 14) and that SW do give the magic numbers 4, 6, and 10. The kind of extensive study performed in Ref. 47 is beyond the scope of this work. However, assuming the same process as in Refs. 47 and 88, we find, for Si_2 - Si_6, that Si_4 is more stable than the other clusters with BH, SW, and T2. PTHT and T3 give more stability to Si_5. With DOD, no cluster shows extra stability as indicated by the almost linear curve in Fig. 6.

All the results presented thus far were obtained with the cutoff function included with the potentials. We have also performed the same calculations with no cutoff; the cutoff function in SW is an integral part of the potential. The two-body potential function without the cutoff function , i.e., $q(r) = V_2(r)/f_c(r)$, is essentially zero at $r = R_c$ for PTHT and BH. $q(R_c)/q(r_e)$ is 0.42, 0.47, and 0.54 for DOD, T2, and T3, respectively. As expected, there is very little or no change in the results obtained with PTHT and BH. For the cluster functionals, there are little changes in the structural parameters, somewhat larger variations in the binding energies (particularly for T3), and some minor changes in the relative position of the minima. The global minimum of Si_4 is now the rhombus for T3 and that of Si_5 is now the flat square pyramid for T2. The largest variations were obtained with T3 but they are not large enough to change the overall picture presented thus far.

Finally, It should be mentioned that, while our results agree with the works of Refs. 20, 28, 46, and 47, there is some conflict with the work of Biswas and Hamann. [10] First, the binding energies listed in Ref. 10 are consistently slightly larger (less than about 0.1 eV/atom) than the values presented here. The structure of Si_3 is in total disagreement; they found an isoceles triangle with $\theta = 79^o$, $r = 2.29$ Å, and $E_B = 5.10$ eV. Our result agrees with that of Ref. 20. With BH, we found all minima reported in Refs. 10 and 20 and many more. Our results for T2 are in agreement with those of Ref. 20 and here again we found other minima.

In summary, the ab initio calculation [88] predicts that, for Si_3 - Si_6, there are overall twelve structures which are minima and seven which are not (there are probably many more than that). Considering these nineteen structures and using a simpler version of the rating scheme of Bolding and Andersen, [20] a potential will predict (m,n) minima with $0 \le m \le 12$ and $0 \le n \le 7$ being the number of correct and spurious minima, respectively. The rating of the ab initio calculation is (12,0). It is (8,4), (8,4), (6,4), (7,5), (7,6), and (6,6) for T2, SW, BH, PTHT, T3, and DOD, respectively. The most serious limitation of these potentials is that they predict many spurious minima which are either global or close in energy to the correct global and local minima. A positive note is that, in general, these potentials do predict, like the ab initio calculations, that the structures derived from crystal fragments are not energetically favorable even though the potentials were built from crystal data. Within the framework of classical interatomic potentials applied to covalently bonded materials, it is the delicate

balance between the radial and bond bending forces which determine the equilibrium structure and the energetics of any system of atoms, e.g., clusters, bulk phases, or surfaces. The fact that these potentials do not describe correctly the equilibrium structures of the silicon clusters indicates that such a balance is not adequate at this point.

5 BULK PHASES

5.1 Crystal Stability

In addition to the cubic diamond structure (a = 5.429 Å; E_c = -4.63 eV/atom), silicon may exist in several simple and complex metastable structures. [89] These phases have been observed experimentally and most of them result from pressure-induced phase transformations. They are: hexagonal diamond which has the same density as cubic diamond (c/a = 1.653 ; a = 3.80 Å), β-tin (c/a = 0.552 ; a = 4.686 Å), BC-8 (x = 0.1003 ; a = 6.636 Å), simple hexagonal (c/a = 0.94 ; a = 2.527 Å), HCP (c/a = 1.698 ; a = 2.444 Å), [99] and FCC. [100] Hexagonal diamond is formed with a combination of high-pressure and heat treatments. [89] The BC-8 structure is observed upon unloading to atmospheric pressure from the high-pressure β-tin phase. [101] The other phases are the result of high-pressure phase transformations in the pressure range 0-800 kbar. [99,100] They occur in the sequence cubic diamond --> β-tin --> simple hexagonal --> HCP --> FCC with increasing pressure.

Accurate DFT calculations have been performed on these structures as well as some other hypothetical phases, e.g., simple cubic, BCC, and graphitic structure. [99] The DFT database has been very useful not only as input for the parametrization of the potentials but also for comparison purposes when experimental data are unavailable as is often the case. To test for crystal stability, and as further comparison between the potentials, we performed calculations for all the structures mentioned above as well as for several two-dimensional structures. The axial ratio, c/a, of hexagonal diamond, β-tin, simple hexagonal, HCP, and graphitic silicon as well as the internal parameter, x, of BC-8 were optimized. The results for the optimized structures are shown in Table IV. In the DFT calculations the c/a ratios of the hexagonal diamond, HCP, and graphitic structures were not optimized. [89,102]

All potentials, but PTHT, predict the cubic diamond phase as the most stable structure. The major result here is the unfortunate finding that with PTHT the lowest-energy phase is the simple hexagonal structure instead of cubic diamond. The axial ratio of 2.87 is so large that there is negligible interaction between the hexagonal layers. The second lowest energy structure is not even cubic diamond but a squared two-dimensional structure with a = 2.32 Å and $\Delta E = E_c - E_c$(cubic diamond) = -0.22 eV/atom. This finding stresses the need, when testing for crystal stability, for considering all plausible phases including planar structures. When PTHT was first developed, crystal stability was tested with a minimum number of structures. [30] This situation is certainly not unique. As an example, the same problem occurred with the first potential developed by Tersoff. [8] Despite this pathology, we will continue in the next sections to present results obtained with PTHT because, as we will show throughout, this potential yields in most cases similar results to those obtained with DOD.

Crystal stability is the first requirement any potential must fulfill for it to be useful. [104] If the potential gives as the most stable structure a phase other than the experimentally observed one, it cannot be used, in general, and particularly for melting and growth simulations. However, it can, perhaps, be used for a limited number of structural calculations in regions of phase space away from the pathological configuration; but one has to remain skeptical of such calculations. When the most stable structures are planar structures, as in the case with PTHT, one can easily foresee situations where the use of such a potential could lead to trouble. For example, in an unconstrained simulation involving (100) or (111) surfaces and where the lateral dimensions are relaxed, the layers making up the slab could break away if the temperature is high enough to overcome the energy barrier preventing bond breaking. In fact, this pathology is perhaps responsible for the results of the simulation of thin amorphous silicon films on crystalline silicon substrates performed by Erkoc, Halicioglu, and Tiller [105] They found that the dominant structural feature was a dense free surface skin with a void layer underneath for Si (100) and (111) substrates.

A good fit to the energy of the hexagonal diamond phase is important because there are direct implications on the energies of stacking faults and of the Si (111) 7x7 surface. The DFT calculation shows that ΔE = 0.016 eV/atom in agreement with the observation that the cubic and hexagonal diamond phases are closely related and with the small experimental stacking fault energies in

silicon along the <111> direction, e.g., 50 - 60 erg/cm^2. [106] BH gives the best fit with a c/a ratio slightly greater than the ideal value in agreement with the experimental value. PTHT gives a vanishingly small ΔE. The other short-ranged potentials, being first-nearest-neighbor models, give, as expected, a zero ΔE.

The BC-8 structure is of particular interest because it provides information about bond-bending forces. This phase has a BCC structure with 8 atoms per unit cell; it has two structural parameters, the cubic lattice parameter, a, and the internal parameter, x. It consists of distorted tetrahedra with small changes in bond lengths. As in cubic diamond, each atom in BC-8 has four neighbors but there are two different types of bonds resulting in two slightly different bond lengths and thus two distorted bond angles, about 99^o and 118^o. [101,107] All potentials describe the structural parameters fairly well; however, with the exception of T2, they overestimate the energy. T2 gives a very small relative energy implying very weak bond-bending forces as already indicated in the previous section. SW, DOD, T2, and T3 correctly predict the bulk modulus; PTHT and BH overestimate it just as they do for cubic diamond (see Table V).

The β-tin structure is also of interest because it is the first phase the diamond structure transforms to under pressure. This phase has four nearest-neighbors and two second-nearest neighbors at a slightly larger distance making the effective coordination number, Z_{eff}, equal to 6. SW gives the best overall description (excluding the bulk modulus). Only T3 correctly predicts the bulk modulus. All but SW, underestimate the c/a ratio and only BH and SW describe the energy fairly well.

The graphitic phase is important because (i) it is the only undercoordinated structure (with respect to cubic diamond) and (ii) it gives a measure of both the tendency of silicon for rehybridization from sp^3 to sp^2 as observed on some surfaces and also of π-bonding which was found by first-principles calculations to be weak in silicon compared to carbon. [102] Note again that in the DFT calculations, the c/a ratio was not optimized. [89] The value of 2.726 for graphite was used. Our results for this value are ΔE = 0.34, 1.09, 1.27, 0.39, 0.70, and 0.72 eV/atom and a = 3.92, 3.99, 4.10, 3.95, 4.01, and 3.99 Å for PTHT,BH, SW, DOD, T2, and T3, respectively. Note the excellent agreement obtained with T2 and T3. The optimized structures, as obtained with these potentials have a much smaller axial ratio of about 1.2, remarkably about the same for all potentials. The energy is also comparable for PTHT, BH, and DOD and for T2 and T3. Z_{eff} is 5 for the atom having neighbors directly above and below in the adjacent layers.

PTHT and BH predict a compressed HCP structure with an axial ratio of 0.59 and 0.69, respectively. In this structure, Z_{eff} is 8 instead of 12 for the ideal HCP structure; this structure is very close in energy to the cubic and hexagonal diamond phases. SW also predicts a HCP structure with a c/a ratio of 0.884, smaller than the ideal value of 1.633; Z_{eff} is only 6 in this case. For the ideal HCP structure the results are a = 2.81, 2.88, and 2.93 Å and ΔE = 0.92, 0.26, and 0.42 eV/atom for PTHT, BH, and SW, respectively. The lower energy of the compressed structure is due mainly, particularly for PTHT, to a lower three-body energy.

The energy of all the structures is compared to the DFT results in Fig. 7. In this figure, the energy of the graphitic structure corresponds to the non-optimized c/a ratio of 2.726. Also, for PTHT, BH, and SW, the energy of HCP corresponds to the ideal c/a ratio. Only DOD shows the same trend in energy (up to the HCP phase) as the DFT results. This is not surprising because Dodson included more structures in the fitting database than the other potentials. PTHT does a poor job in describing the energy of these phases. Only SW, DOD, T2, and T3 predict the BC-8 structure as the next-lying phase after cubic and hexagonal diamond, and only SW and DOD predict β-tin as the fourth phase. All potentials correctly predict that the equilibrium atomic volume of cubic diamond is larger than that of the other phases (excluding the non-optimized graphitic structure). They also predict the increase of bond length with increasing coordination (the dependence is approximately logarithmic). However, the bond lengths are, in general, somewhat larger (particularly with SW and BH) compared to the DFT results.

5.2 Phase Transformations

As a further test and comparison, we finally discuss pressure-induced phase transformations. We have studied all possible phase transformations (mainly from the cubic diamond structure to all the other bulk phases) using the procedure outlined in Ref. 89. Only T3 predicts correctly that cubic diamond will first transform to the β-tin phase at a transition pressure of 127 kbar. The transition volumes (normalized to the experimental equilibrium volume of cubic diamond) are 0.903 (cubic diamond) and 0.715 (β-tin). This agrees fairly well with the experimental values of 88-125 kbar, [108] 0.918, and 0.710, [89] respectively. T3 also predicts a β-tin to BC-8 transformation at 47 kbar compared to the DFT

result of 76 kbar. [101] The first transformation from cubic diamond is predicted to be to the compressed HCP phase by PTHT and BH, to BC-8 by SW and T2, and to simple hexagonal by DOD. The cubic diamond to β-tin phase transformation is predicted to be (in the order of increasing transition pressure) the third transformation by PTHT (286 kbar, 0.93 (cubic diamond), 0.77 (β-tin)), the fifth by BH (155, 0.93, 0.84), the second by SW (217, 0.86, 0.82), the fourth by DOD (205, 0.85, 0.76), and the fifth by T2 (270, 0.84, 0.73). Biswas and Hamann [10] found that cubic diamond would make a transition under pressure first to simple cubic. We found this transition to occur after the cubic diamond to HCP transition using their potential.

5.3 Elastic and Vibrational Properties

The description of the elastic properties (in particular, the shear constant C_{44}) constitutes a stringent test for the potentials. We have calculated the elastic constants using the homogeneous deformation method. [84] The results are presented in Table V. The cluster functionals were all fitted to the bulk modulus, B; it is thus well described. They also descibe well the pressure derivative of the bulk modulus, B'. SW provides a good fit to B but significantly underestimates B'. PTHT and BH overestimate C_{11}, C_{12}, B', and B. DOD and T2 underestimate C_{11} by about 28%; SW and T2 overestimate C_{12} by about the same amount. All potentials underestimate C_{44}; the worst fit is provided by T2, PTHT, and BH. For T2, this indicates once again the very weak bond-bending forces. Note that they also underestimate the second shear constant (C_{11} - C_{12}). Also, none of the potentials correctly describe the negative Cauchy discrepancy (C_{12} - C_{44}). PTHT and DOD overestimate significantly Kleinman's internal strain parameter, ζ. [23] This is reflected in the large value of (C^0_{44} - C_{44}). C^0_{44} is the value of C_{44} in the absence of internal displacement. [110] BH, SW, and T3 provide a good fit to C^0_{44} and ζ. This shows that such a good fit does not necessarily result in an accurate value of C_{44}. Tersoff developed T3 in order to improve on the elastic constants. T3 indeed describes the elastic constants better than does T2. SW also gives a good description. This is in fact quite remarkable considering that SW was not directly fitted to any elastic constants. For all potentials, the elastic constants satisfy the mechanical stability conditions indicating that the cubic diamond structure is stable against all elastic homogeneous deformations. [84]

The vibrational properties influence small distortions from equilibrium and are thus also important. In Table V are listed the phonon frequencies corresponding to four modes, the transverse acoustic at X, TA(X), the transverse optic at X, TO(X), the longitudinal optic and acoustic at X, LOA(X), and the longitudinal-transverse optic at Γ. The phonon spectrum for DOD is not available. BH gives the best overall description of these phonon frequencies. [10] For PTHT, despite a very poor description of the elastic constants, the phonon frequencies agree fairly well with experiment with the exception of $\nu_{TO}(X)$. Note the almost perfect agreement for $\nu_{TA}(X)$. The full phonon spectrum has been determined by Pearson. [34] At the zone boundary, the acoustic modes are well described. However, the optical modes are too stiff; besides a larger zone center frequency, the modes increase with increasing wave vector, instead of decreasing. The fact that PTHT and BH give a better agreement with experiment for the transverse acoustic mode at X than the other shorter-range potentials is consistent with the observation that long-range interactions are necessary for an adequate description of this mode. [113] While SW also does a fairly good job with these phonon frequencies, the spectrum extends to higher frequency compared to experiment. T2 gives a poorer overall description of the phonon spectrum than SW. $\nu_{TA}(X)$ is underestimated significantly. [27] T3 gives a description comparable to SW. [13]

5.4 The Universal Energy Relation

All properties of the cubic diamond structure presented thus far probe only a very small region around equilibrium. It is desirable to seek information about the behavior of the potentials in regions well away from equilibrium. Recently, Rose, Smith, Guinea, and Ferrante [114] showed that the binding energy versus distance relation for a condensed system, independent of its bonding character, could be described by a universal energy relation (UER) given by,

$$E(a^*) = E_c\,(1 + a^* - f_3\,a^{*3})\,e^{-a^*}$$

Where $a^* = \eta(r/r_e - 1)$ and $\eta = (9B\Omega_e/|E_c|)^{1/2}$. Here r is the first nearest-neighbor distance and Ω is the atomic volume while the subscript e indicates equilibrium values. The coefficient f_3 was fixed to a value of 0.05 which was determined from the thermal expansion of copper. [114] This led to a value of 4.74

for B' in silicon compared to 4.2 for the experimental value. A value of 0.0052 for f_3 leads to an exact fit whereas $f_3 = 0$ gives B' = 4.25; f_3 was set to zero in this work. In general, good agreement was found between the universal energy relation and experimental data as well as the first-principles calculations. The UER not only accurately models the region of moderate uniform compression but it also provides information about the behavior of the crystal under moderate uniform expansion where experimental data is lacking.

The energy versus distance curves are shown in Fig. 8. Compared to the UER curve, BH and PTHT indeed do a poor job. The repulsive branch of the curve is well described by the short-range potentials. The cluster functionals also do a good job for expansion up to a bond length of about 2.8 Å. Note that the UER suggests that the potential is long-range; however, the accuracy of the UER has not been demonstrated for large expansions. According to first-principles calculations, [83] the range of the two-body potential is about 5Å (see Fig. 2). Moreover, the many-body term should fall off much more rapidly with distance than the two-body term. It thus seems reasonable to assume that the range of the potential should be no more than about 5 Å.

To further characterize the behavior of the energy-distance curve, we consider a theoretical property defined in Ref. 114 as a limit on the tension at which the crystal would rupture. This negative pressure, P_R, is the value at the minimum of the pressure versus distance equation. It was found that, for most crystals, P_R is typically 10 to 20% of the bulk modulus. Compared to the UER value of -0.16 Mbar, P_R is -0.17, -0.14, -0.16, -0.34, -0.36, and -0.53 Mbar for PTHT, BH, SW, DOD, T2, and T3, respectively. The corresponding strain, ε_R, is 9, 13, 20, 26, 26, and 20%, respectively while the UER value is 15%. The large overestimate of P_R and ε_R exhibited by the cluster functionals is due entirely to the short range and abrupt cutoff (Figs. 2 and 8).

5.5 Bulk Point Defects

In general, point defects involve large atomic displacements and rebonding around them. They provide information about bond-breaking energies and are important for testing the ability of the potentials to model such large atomic displacements. Several calculations or simulations of intrinsic defects were previously performed using BH, SW, T2, and T3. Using SW, Batra, Abraham, and Ciraci [50] performed an extensive molecular-dynamics simulation (at zero

pressure and temperature and in a cell containing 800 atoms) for four types of self-interstitials: the tetrahedral (I_T), the hexagonal (I_H), the bond-centered (I_B), and the dumbbell or split (I_S) interstitials. Biswas and Hamann [10] calculated the energy of formation of I_T, I_H, and the vacancy. Tersoff, using T2, [12] calculated "upper bound" values for the energies of I_T, I_H, I_B, and the vacancy; with T3, [13] he reported energies for the same defects and also for I_S, I_X, the split vacancy and the saddle point for the concerted exchange mechanism of Pandey. [115] Using the procedure outlined in Sec. 3, we have performed our own calculation for I_T, I_H, I_B, I_S, the vacancy, and the split vacancy. We have calculated defect energies at constant atomic volume ($\Omega = \Omega_e$) and at constant pressure ($P = 0$). The volume relaxation reduces the formation energies by less than 0.1 eV. This is because our cell is very large and extends to the 24th shell from the defect. For a (64 ± 1) atoms cell, volume relaxation is more important and reduces the formation energies by up to 0.3 eV. The formation energies of the equilibrium (relaxed) configurations presented in Table VI include volume relaxation, i.e., they are formation enthalpies at zero pressure. There is no reliable experimental data for the equilibrium energies and structures of these defects; therefore, our results are only compared to those obtained with first-principles methods. As indicated in Sec. 3, there are, however, large uncertainties in these ab initio data so that only a range of values is really available at this time. These are also listed in Table VI.

PTHT understimates significantly the energies of all the defects, in particular I_T and the vacancy. The short-range potentials give a better description of the energy of I_T than the longer range potentials (PTHT and BH). This would confirm the observation of Biswas and Hamann that short-range functions are needed to model such a defect. [10] In fact the short-range potentials (T3, SW, DOD, and T2 in that order) appear to give a better overall description of the energies of all defects considered here.

PTHT gives a small relaxation of the nearest neighbors surrounding I_T. With all potentials, I_T has four and six first and second neighbors at 2.44 and 2.8 Å (PTHT), 2.54 and 2.84 Å (BH), 2.56 and 2.94 Å (SW), 2.57 and 2.69 Å (DOD), 2.52 and 2.72 Å (T2), and 2.38 and 2.96 Å (T3). I_H has six first neighbors at 2.42 Å (PTHT, DOD, and T2), 2.51 Å (BH), 2.58 Å (SW), and 2.48 Å (T3). I_B has two first neighbors at 2.36 Å (PTHT), 2.63 Å (BH), 2.31 Å (SW and DOD), 2.27 Å (T2) , and 2.23 Å (T3). The two atoms forming I_S are separated by about 2.19 Å (SW) - 2.33 Å (PTHT). They each have two second neighbors at

2.28 Å (T3) - 2.36 Å (SW). In general, all potentials confirm the findings of Batra, Abraham, and Ciraci [50] that (i) there are significant atomic relaxations extending to several shells around the defect and (ii) the relaxation is oscillatory in nature and somewhat nonuniform within some shells.

BH and SW lead to an equilibrium configuration of the vacancy where the neighboring atoms relax radially (along ⟨111⟩) inward towards the defect. This relaxation brings the surrounding atoms (initially separated by 3.84 Å) closer to each other to about 2.89 Å resulting in a weak interaction of their dangling orbitals. It also increases the length of the back bonds to 2.44 Å. We note that for SW, the ideal configuration is metastable (see Sec. 6.1.1). Biswas and Hamann reported that the relaxation energy for the vacancy was zero. We found that, unlike for SW, the ideal configuration is not at equilibrium because the forces on some atoms although small are quite significant. PTHT, DOD, T3, and T2 give an outward relaxation (also along ⟨111⟩) in analogy with the (111) 1x1 surface. In fact, the amount of relaxation correlates somewhat with the first interlayer contraction of that surface (see Table VIII). With PTHT, DOD, and T3, there is another metastable configuration for the vacancy where the relaxation is inward. In this case, the vacancy formation energy and the fractional amount of relaxation are 2.87 eV and -31.5% (PTHT), 4.21 and -32.2 (DOD), and 4.00 and -28.9 (T3).

Whether the relaxation around the vacancy is inward or outward is still a subject of controversy. Most past quantum-mechanical calculations lead to an outward relaxation (see Ref. 96 for a discussion of such work). More recently Kelly, Car, and Pantelides [96] found an inward relaxation of about 0.2 Å compared to 0.6 Å and 0.56 Å for BH and SW. Antonelli and Bernholc [95] also found an inward but smaller relaxation (-2.8%). Wang, Chan, and Ho [116] using a tight-binding molecular-dynamics method also arrived at an inward relaxation of 0.5 Å which compares very well with the results obtained with BH and SW.

The configuration corresponding to the split vacancy is the classical saddle point for vacancy migration. In this migration path, a neighboring atom moves along a bond and displaces the vacancy. The saddle point is expected to be the configuration where the atom is at the mid-bond site. This atom has six first neighbors at about 2.96 Å when these are at their ideal positions. The ab initio results [96] for this defect are: E_f = 5.01 eV (unrelaxed) and 4.19 eV (relaxed), and an inward relaxation of the six neighbors of 0.28 Å. The calculation of the

vacancy formation energy lead to 4.5 and 3.92 eV for the unrelaxed and relaxed configurations, respectively. [96] The resulting migration energy for the vacancy is 0.27 eV compared to the experimental value of 0.45 eV. We note that both Tersoff potentials give the split vacancy as the most stable configuration for the monovacancy. The inward relaxation of the neighbouring atoms is described well by T3, SW, and BH. Assuming, as in Ref. 96, that the configuration of the split vacancy is the saddle point for vacancy migration, the migration energy for the vacancy as obtained with BH and SW is 0.18 and 0.54 eV, respectively. We note the excellent agreement with experiment provided by SW.

Our results obtained with SW agree with those of Ref. 50. For T2, only the result for the vacancy agrees with that of Ref. 12. For I_T, I_H, and I_B, our results for E_f are consistently smaller but, as indicated above, Tersoff stated that his numbers were upper bounds on E_f. Also our values for the formation energy of I_T obtained with T3 is smaller by 0.35 eV than Tersoff's result. [13] The largest discrepancies are with the relaxed formation energies of I_T and I_H obtained with BH. Biswas and Hamann [10] reported values of 3.61 and 5.09 eV, respectively, compared to our results of 1.56 and 2.89 eV. On the other hand the unrelaxed formation energies are in much better agreement: 4.99 and 9.47 eV compared to our numbers 4.57 and 9.31 eV. Our result for the unrelaxed vacancy formation energy is exactly the same as theirs. Biswas and Hamann did not specify clearly the cutoff radius and size of the cell they used for the defect calculations. To try to resolve this question, we performed calculations for these two defects with a small cell containing 65 atoms and used different values for the cutoff radius, R_C. With R_C = 5.0 Å, there is very little change in the results of Table VI. With R_C = 3.95 Å, the formation energies are 0.83 eV (4.86 eV, unrelaxed) for I_T and 2.57 (9.73) for I_H. Finally, with R_C = 3.0 Å, we found 4.35 (9.74) and 5.56 (14.46), respectively.We do not know at this time what is the reason behind these differences. We do believe that our results are correct.

5.6 The liquid and amorphous states.

We have not performed any simulation of liquid (*l*-Si) or amorphous (*a*-Si) silicon; however, numerous studies have been performed by others to study these two bulk phases. For *a*-Si, the resulting structures seem to be very much dependent on the simulation procedures. [52-54] Also, the potentials were sometimes altered in order to achieve a better description of the amorphous

state. [43] For these reasons, we will not attempt to review the simulation work done with BH, SW, T2, and T3. Instead, the interested reader is directed to the original literature given for each potential in Sec. 2.

Takai, Halicioglu, and Tiller performed a constant pressure Monte Carlo simulation to study the melting of silicon using the PTHT potential. [33] The melting temperature, T_m, was determined to be about 1920 K in fair agreement with the experimental value of 1685 K. The potential correctly describes the volume contraction upon melting; however, other properties of *l*-Si such as the latent heat of fusion are 2 to 3 times smaller than the experimental values. The structural properties were not reported.

Because a requirement in the fitting procedure was to accurately reproduce the melting point of the crystal and the structure factor of the liquid, [6] SW gives the best overall description of *l*-Si than any other potential. Several groups studied *l*-Si and *a*-Si using this potential and different simulation methods. [6,51-53,55,62,67-68] Stillinger and Weber determined T_m to be about 2013 K. [6] However, all other studies lead to a value in the range 1665 - 1750 K. The structure of *l*-Si is also rather well described and other properties are in good or fair agreement with experiment.

BH and T3 strongly overestimate T_m which is about 2900 K [43,44] and 3000 K [13], respectively. The radial distribution function of the liquid is described fairly well by T3. T2 does not describe *l*-Si well. [12] Both Tersoff potentials seem to favor four-fold coordination in the liquid in disagreement with experiment.

Note that the simulations of *l*-Si reported here for PTHT and SW were performed with the original sets of energy parameters. These parameters, as indicated in Sec. 2, give a bulk cohesive energy, E_c, of diamond silicon of -5.45 eV for PTHT and -4.34 eV for SW. Simulations on melting have predicted strong correlation between T_m and E_c. [117] Thus we may scale T_m with E_c and the results for PTHT and SW become 1631 K and 1776 - 1867 K, respectively.

6 SURFACES

In view of the rich variety of surface reconstructions they exhibit, surfaces of silicon represent, perhaps, the most stringent test for the potentials. We consider in this section the low-index (100), (111), and (110) surfaces. Because of their technological importance in the microelectronics industry, the (100) and (111) surfaces of silicon have been extensively studied both experimentally and

theoretically over the last 30 years. A myriad of experimental techniques were used to determine their geometrical and electronic structure. Several models have been proposed and many theoretical studies, most notably self-consistent total-energy pseudopotential calculations, have been performed to explain the different surface patterns observed. For a complete review of these surfaces the reader is referred to the articles of Haneman. [118] It is worthwhile to note that experimental observations of these surfaces are made at $T \neq 0$. Temperature effects associated with the entropy can therefore be important and might be the critical factor responsible for the relative stability of some surfaces, e.g., Si(100) and Si(111) 7x7. However, because calculations or even estimates of the entropy are difficult, we use, as is common, zero temperature surface energies to study the stability of such surfaces.

6.1 Si(100)

Despite its apparent simplicity, the Si(100) surface has long been the subject of controversy. Many models have been proposed over the years to explain the various surface patterns observed experimentally. [119,120,121] It is now universally accepted that the dimer model is the correct one. The dimerization of the Si(100) surface has been particularly confirmed by STM observations in real space [120,122] and also by numerous total-energy calculations, principally those using first-principles pseudopotential techniques. [86,90,123-126] The reduction of the dangling bond density is the primary driving force for the dimer reconstruction. Dimerization occurs when two surface atoms (initially in their ideal bulk positions and separated by the second neighbor distance of 3.84 Å), which have two dangling bonds per atom, move toward each other in the [110] direction and in the plane containing their dangling bonds to form a bond. This is illustrated in Fig. 9 which shows symmetric dimers. The dimerization induces subsurface atomic displacements which extend at least four layers into the bulk. The dimer is buckled and asymmetric when the dimer atoms have different x and z displacements from their ideal bulk positions. The x and y directions, taken as [110] and $[\bar{1}10]$, run along the dimer bond and the rows of dimers, respectively.

Both 2x1 and c 4x2 patterns have been observed in LEED and He-atom diffraction experiments; the latter also showed the presence of p 2x2 and possibly c 2x2 patterns. [119] The situation was clarified recently by Tromp,

Hamers, and Demuth who used an STM with a lateral resolution of about 3 Å to determine the atomic structure of the clean Si(100) surface. [123] They only observed asymmetric buckled and symmetric nonbuckled dimers along with a relatively high density (approximately 10%) of dimer vacancies. The surface defects, which are randomly distributed, appear as both individual dimer vacancies and small clusters of missing dimers. No other type of reconstruction was observed. The density of buckled and symmetric dimers is nearly the same indicating that their energies are approximately equal. This is supported by ab initio calculations as we will see below. [90,124,125] In defect-free regions, the dimers are symmetric and the periodicity is 2x1. The buckled dimers, which give rise locally to p 2x2 and c 4x2 patterns, are often observed near vacancies and at steps. This suggests that the surface defects induce or at least stabilize buckling. [120] The p 2x2 and c 4x2 structures are formed by alternating the buckling along a row of dimers for both of them but, in adjacent rows, the buckling is parallel and antiparallel for the former and latter, respectively. The c 2x2 structure was not observed.

In this work, the Si(100) surface is modeled with a slab containing 20 layers of 16 atoms each. The top 14 layers are allowed to relax while the rest are held fixed. The cartesian coordinate system is shown in Figs. 9 and 10. For the dimer reconstruction, the surface atoms are initially displaced toward each other to form dimers. The results for the ideal and relaxed 1x1, the dimer reconstructed 2x1 and c 2x2 surfaces, and the Pandey π-bonded defect structure are presented and compared to the DFT results in Table VII.

6.1.1 Si(100) 1x1

The energy of the ideal 1x1 surface, as obtained with the six potentials, is comparable to the DFT result of 2.5 eV. This value obtained at 4.3 Ry is probably an upper bound. The largest discrepancy is obtained with PTHT and DOD which give about the same value. By relaxing the 1x1 surface, the energy is slightly lowered in agreement with the DFT result. This relaxation, of both energy and first interlayer contraction, is perfectly described by BH and to a lesser extent by T3. Again, PTHT and DOD produce similar results; they both overestimate the relaxation energy by about a factor of 3. DOD gives an interlayer contraction of 10%, twice the DFT result. T2 gives very little relaxation. In the case of SW, all stresses are zero and the surface exhibits no

relaxation; this is true, as we will see later, for any bulk terminated surface or any defect that is created by removing atoms, e.g., vacancies. This behavior can be directly related to the form of the potential [37,58] and is explained by the combined effect of three features: (i) the potential includes only first-neighbor interactions, (ii) the total 3-body energy vanishes at the tetrahedral angle, and (iii) the Si_2 molecule bond length and strength are exactly equal to the bulk equilibrium bond length and energy. As a result of (i) and (ii), the forces and all stresses on all atoms are zero; consequently, the ideal 1x1 structure of any surface is a minimum on the potential energy surface. There is no relaxation (for unreconstructed surfaces) because of (iii). Compared to the DFT results, the potentials do not, in general, predict the surface stress well. For the ideal 1x1 surface, they all underestimate σ_{xx}; the short ranged potentials even predict a zero stress for that direction. PTHT and BH overestimate σ_{yy} strongly; T3 predicts a negative value.

6.1.2 Dimer Reconstruction

Since we will compare our results with those obtained via ab initio methods, it is worthwhile to review those theoretical calculations. As stated above, numerous total energy calculations were performed over the years in an attempt to explain the experimental observations. [86,90,118,123-126] We only focus on three of them which all used the pseudopotential technique.

Pandey [124] found that the lowest energy configuration in a 2x1 cell leads to symmetric dimers. The surface energy (relative to the ideal 1x1 surface), computed with Epw = 6 Ry, is -2.06 eV/dimer. Pandey also showed that, using this minimum energy structure and buckling the dimer such that no bond length is altered, the energy was raised by 0.02 and 0.11 eV/dimer for a tilt angle (with respect to the surface) of 10^o and 15^o, respectively. Batra [90] also obtained symmetric dimers for his optimized 2x1 surface with a relative energy of -2.34, -2.06, and -1.86 eV/dimer at 5.5, 6.5, and 7.5 Ry, respectively. Note that this indicates that the surface energy has not yet fully converged. An optimized buckled geometry with 2x1 symmetry and a tilt angle of 8^o raised the energy by only 0.02 eV/dimer at 7.5 Ry. However, buckled dimers in 2x2 symmetry lowered the energy by 0.0054 eV/dimer (this structure was not optimized and the buckling was very small). Batra also showed that there is no barrier to dimerization and that twisting of the dimers is energetically unfavorable. Roberts

and Needs [125] performed what is perhaps the most extensive calculation of dimer reconstruction on the Si(100) surface. They considered different geometries including the 2x1 surface with symmetric and buckled dimers, the p 2x2 structure with alternating buckled dimers, and other structures with missing dimer defects. They found that buckled dimers have lower energy than symmetric dimers. The relative energies, obtained at 6 Ry, for the buckled p 2x2 and 2x1 structures and the symmetric 2x1 structure are -2.108, -2.078 and -2.02 eV/dimer, respectively. The energy difference is indeed small and is comparable to the accuracy of their calculation. In fact, the energy difference between the buckled and symmetric dimer in the 2x1 structure is only 0.03 eV/dimer at 10 Ry. The buckled dimer in the 2x1 structure is tilted by about 6.9^{o} while the two alternating buckled dimers in the 2x2 cell have different tilt angles, 11.6^{o} and 12.3^{o}. For the optimized 2x1 structure, the structural parameters are nearly the same for the three calculations. They are given in Table VII and Fig. 9. The main results from these calculations are (i) the symmetric and buckled dimers have nearly the same energy which is compatible with the observation that they have nearly the same density, (ii) the dimers are not twisted, (iii) the dimer bond length is shorter than the bulk bond length indicating multiple bonding character, and (iv) the back bonds are strengthened.

For all potentials, the Si(100) surface reconstructs to form symmetric dimers. Twisting the dimers raised the energy in agreement with the DFT result. No potential is able to model buckling which is a quantum-mechanical phenomenon. [123,128] This will probably require inclusion of atomic interactions higher than three-body in the potential and even possibly fitting the potential parameters to a buckled structure. Both the 2x1 and c 2x2 structures are found to be stable with a small energy difference between them. Only PTHT and DOD incorrectly predict that the c 2x2 surface is more stable. For PTHT, the energy gain of the c 2x2 structure over the 2x1 structure is due to a lower two-body energy, the three-body energy being about the same, while for DOD, it is due to a lower three-body energy (positive) despite the increase of the negative two-body energy. The structural parameters (bond lengths and angles) are nearly the same for both structures, which is consistent with their small energy difference.

We now focus on the 2x1 reconstruction. Note that, as indicated above, the DFT value of -0.93 eV for the relative energy of this surface is certainly a lower bound. Thus, all potentials, but T2, lead to a surface energy in fair agreement with the DFT result. Only PTHT, DOD, and T2 give a dimer bond length smaller

than the bulk equilibrium bond length (2.352 Å). The value for T3 is very close; the largest discrepancy is obtained with BH and SW. For the back bonds between surface and second-layer atoms, the DFT calculations show a strengthening with a length slightly larger than the dimer bond length. Only PTHT, DOD, T2, and T3 give this back bond strengthening. Also, only for T2 is the length of these back bonds larger than that of the dimers. Note, however, that all bond lengths are within 2% of the bulk bond length and that the largest discrepancy between the DFT results and those obtained with the potentials is 7, 3, and 5% for the dimer bond length, the length of the back bonds, and the bond angles, respectively.

According to the DFT calculation, the ideal 1x1 surface is under a strong tensile stress along the eventual dimerization direction and under a weaker tensile stress in the perpendicular direction. The reduction of σ_{xx} after dimerization suggests that stress relief is the driving force for the dimer reconstruction. However, if this were the case, σ_{yy} would also be small; but it is now stongly compressive. Therefore, just as for the Si(111) 7x7 structure, [85] it is primarily the reduction of the dangling bond density that stabilizes the dimer reconstruction on the Si(100) surface. Only SW and T3 predict the correct sign for the two stresses. SW overestimate σ_{xx} by 68% and gives a vanishingly small σ_{yy} while T2 underestimate both of them by 47 and 36%, respectively. BH and T2 predict the value of σ_{xx} very well but both give a positive σ_{yy} (almost zero for BH). On the other hand, PTHT and DOD predict σ_{yy} very well; they, however, predict a compressive stress in the x-direction. It is worthwhile to indicate that, for all potentials (even those for which the sign of one of the stresses is wrong), the 2x1 surface is more compressed (less tensile) in the y-direction than it is in the x-direction.

6.1.3 Surface Defects

We now turn our attention to the surface defects. It does appear that the high defect density is intrinsic of the (100) surface. Indirect support for this is provided by the observation that similar sample preparation procedures for (111) surfaces lead to a low surface defect density [120] and by the low formation energy of dimer vacancies. [125] On the other hand, the geometrical arrangement of the defects depends on the sample preparation technique and/or the presence of impurities on the surface. In the STM experiments, [120,123] the samples were

gradually cooled down after annealing at high temperatures, this led to a random distribution of missing dimers. In another STM experiment, [129] missing dimer defects ordered along the dimerization direction are clearly seen when small amounts of gallium are deposited on the Si(100) surface. Indirect evidence for ordered dimer vacancies is also provided by the LEED studies of higher-order periodicities which can be produced by rapid quenching from high temperatures. These are c 4x4 and c 8x8 [130] and, in particular, 2xn with $6 < n < 10$. [131] These structures have all been explained with models involving ordered dimer vacancies. For the 2xn structures, it has been determined that they are metastable and that quenching at higher rates or from higher temperatures lead to small n. [131] It is clear from the above that dimer vacancies play an important role in the energetics and structures of the Si(100) surface. For the potentials to be useful, it is essential that they give at least a reasonable description of such defects. Roberts and Needs [125] calculated the surface energy of the Pandey π-bonded defect structure. [124] In this model, shown in Fig. 10, a dimer vacancy is created at every fourth site along the rows of dimers. This leads to a structure with 2x4 symmetry. In the DFT calculation, the structure was optimized but the dimers were not allowed to buckle. Its energy is only 0.035 eV/1x1 cell higher than that of the 2x1 symmetric dimer reconstruction. This corresponds to a formation energy (with respect to the 2x1 symmetric dimer structure) of 0.28 eV/defect. In a 2x2 cell, where the dimer vacancy concentration is 0.5, the formation energy is 1.10 eV/defect. Clearly these surface defects repel each other. Now, while the creation of a dimer vacancy induces strain in the surface, it does reduce the dangling bond density by rebonding of the exposed second-layer atoms. Thus, the optimum surface defect concentration is probably lower than 0.25 and is a compromise between the two effects.

The results of our own calculation for this defect structure are presented in Table VII. DOD considerably overestimates the strain energy and leads to a surface energy only slightly lower than the ideal 1x1 surface. At the other end, T2 predicts that vacancy formation is exothermic (with respect to the 2x1 structure) in agreement with Pandey's predictions (Pandey [124], who did not perform a calculation, estimated that the defect would lead to a large energy gain of 2.0 eV/defect which seems quite unreasonable). BH , SW, and T3 do predict that the defect structure is metastable and give results in fair agreement with those of the DFT calculations. While, as stated above, the potentials do not, in general, give a good description of the surface stress, it is worthwhile noting

that, qualitatively, the surface defects induce atomic displacements such that the tensile stress along the dimer bonds is reduced and that the surface is now under tension (or at least under less compression) in the y-direction. The atomic displacements are qualitatively similar to those of the DFT optimized structure. Only DOD predicts a shortening of the bond length of the dimers adjacent to the defect; the others predict a small expansion ($\leq$ 1%). The length of the weak bond formed by the exposed second-layer atoms is 2.562, 2.625, 2.318, 2.871, and 2.656 Å for BH, SW, DOD, T2, and T3, respectively compared to the DFT result of 2.71 Å.

In conclusion, BH, SW, T3, and to a lesser extent T2 give a reasonable description of the energetics and structures of the Si(100) surface whose principal features are the dimerization of the surface atoms and the existence of dimer vacancies. This is mainly due to the fact that the angular distortions (from the tetrahedral angle) on this surface are relatively small (about $\pm$ 12% for the 2x1 surface; they are somewhat larger for the defect structures), at least compared to those encountered in small clusters and on the (111) surface. Their principal limitation is the inability to model buckling which might not be serious because the energies of the buckled and symmetric dimers are nearly degenerate. Clearly surface defects play an important role here and any realistic calculation or simulation which aims to study them will have to involve systems with a large number of atoms. Powerful and accurate first-principles methods, such as the now widely-used ab initio molecular dynamics technique, [132] are still limited to studies of relatively small systems (up to 150 atoms [133]). It is believed that the potentials mentioned above will be useful in large-scale simulations of the Si(100) surface since they predict its properties reasonably well and they can handle large systems with atoms in the tens of thousands. [60]

6.2 Si(111)

The Si(111) surface exhibits several reconstructions depending on the purity of the surface, the temperature, and the sample preparation procedures. We consider here only clean surfaces. A freshly cleaved (111) surface in UHV reconstructs to form a 2x1 metastable structure which transforms irreversibly upon heating (the transition temperature ranges from 200 to 350 ^{o}C depending on the step density [134]) to the stable 7x7 phase which, in turn, transforms

reversibly to a structure with 1x1 symmetry at about 830 °C. This 1x1 phase, which still remains a mystery, [118] is not the bulk terminated surface.

The widely accepted model for the 2x1 surface is the Pandey π-bonded chain model. [85,91,132,135-138] This structure is similar to the (110) surface. Another interesting model, called the three-bond-scission model, has been recently proposed by Haneman. [118,139] For the 7x7 surface the DAS model of Takayanagi, Tanishiro, Takahashi, and Takahashi is now universally accepted. [140-144] Other metastable structures have also been observed. STM experiments on (111) surfaces prepared by a combination of laser and heat treatment showed locally the existence of 2x2, c 4x2, $\sqrt{3}$x$\sqrt{3}$, 5x5, and 9x9 structures. [145] The first three have been explained by simple adatom covering of the surface with the adatom located in the T_4 site. The (2n+1)x(2n+1) structures were explained with DAS type models. [144-146] A $\sqrt{3}$x$\sqrt{3}$ structure has also been observed in a LEED experiment; [147] the LEED data were fitted to a vacancy model which was shown to be energetically unfavorable. [37,148]

We have performed calculations for most of the structures mentioned above. In general, the Si(111) surface was modeled with a slab containing eight double layers. The top four or five double layers were allowed to relax while the rest were held fixed. The orthogonal x and y surface axes run along the $[1\bar{1}0]$ and $[11\bar{2}]$ directions, respectively. Depending on the symmetry of the surface, the number of atoms per layer ranged from 24 to 162 corresponding to a total number of moving atoms of 240 to 1640, respectively. The surface energies and stresses for the (111) surfaces are presented in Table VIII.

6.2.1 Si(111) 1x1

Compared to the DFT result, the surface energy of the ideal 1x1 surface is underestimated by all potentials. Although bond breaking energies are certainly important, only the relative energies are relevant when investigating the stability of one surface structure over another. We note that the relaxation of the 1x1 surface is best described by PTHT, DOD and T3; however, they all significantly overestimate the compressive lateral surface stress. With BH and T2, the 1x1 surface exhibits little relaxation resulting in a small tensile stress. As indicated above, in the case of SW, all stresses are zero and the surface exhibits no relaxation. As expected, all short-ranged potentials predict a zero surface fault

energy for the 1x1 faulted surface. PTHT and BH give a value of 0.012 and 0.015 eV/1x1 cell compared to the DFT result of 0.02 to 0.06 eV.[91] They, however, predict a surface stress of -2.31 and -0.04 eV/1x1 cell while the DFT value is 0.11 eV/1x1 cell.

6.2.2 Si(111) 2x1

Using a cleavage technique, Gilman[150] measured the surface energy of the (111) surface at 77 K. He obtained a value of about 1 eV/1x1 cell. Since, as indicated above, a freshly cleaved surface transforms to a 2x1 reconstruction, except for any generated strain energy associated with the cleavage process, this value can thus be taken as the experimental surface energy of the (111) 2x1 π-bonded surface. The DFT result of 1.11 eV compares very well with this value.

Only PTHT predicts that the 2x1 π-bonded structure is stable with respect to the ideal 1x1 surface. the relative energy is however underestimated by a factor of 3. Moreover, the DFT calculations predict that the structure is also buckled.[132,135,137,138] Again the potentials cannot model buckling. For BH, this structure is not even a minimum. The 2x1 surface reduces its energy by π-bonding of the surface dangling bonds which are now first neighbors instead of second neighbors as they are on the 1x1 surface. Since the potentials do not model π-bonding, for them the dangling bond density is unchanged. Therefore, there is no energy gain to overcome the strain energy caused mainly by angular distortions ($\pm$10%). Only for PTHT is this strain energy compensated by a strengthening of the bonds in the surface chains. DOD shows a somewhat similar behavior, but the strain energy is higher due to a stronger three-body energy (Fig. 4). Our result for DOD is in disagreement with that of Dodson who reported that the 2x1 reconstruction reduces the energy of the (111) surface by 0.12 eV/1x1 cell.[9] In general, the potentials predict that the 2x1 surface is under a weak and stronger tensile stress in the directions parallel and perpendicular to the chains , respectively; the DFT calculation predicts the opposite.[85] However, the comparison here is not truely appropriate because the DFT structure is buckled and stresses are more sensitive to the atomic displacements than is the energy.

6.2.3 Adatom Structures

According to the DFT calculations,[91] all adatom covered structures are stable (with respect to the ideal 1x1 surface) in the order 2x2 T_4 < $\sqrt{3}$x$\sqrt{3}$ T_4 < 2x2 H_3 < $\sqrt{3}$x$\sqrt{3}$ H_3. Thus, the 2x2 structure is more stable than the $\sqrt{3}$x$\sqrt{3}$ structure in spite of the fact that it has a smaller reduction of the dangling bond density. The energy difference is, however, only 0.06 eV/1x1 cell. Meade and Vanderbilt have attributed the energy lowering to the different electronic structure of the two surfaces.[91] Note that, with the same adatom concentration of the 2x2 structure, two different structures with rectangular c 2x4 and c 2x8 symmetries can be generated.[146] We have not considered these structures in this work. Before we discuss the results for the adatom structures, note that there are four errors in Table I of Ref. 37. For T3, the relative energy of the relaxed 1x1 surface should be -0.07 and the energy and stress of the $\sqrt{3}$x$\sqrt{3}$ H_3 surface must be 0.482 and -0.522, respectively. The surface stress of this latter structure should read -0.502 for BH. Also, our calculation with SW for the $\sqrt{3}$x$\sqrt{3}$ structures do not agree with that of Ref. 27. Li, Chen, Allen, and Broughton reported 1.53 and 1.82 eV/1x1 cell for the surface energy of the $\sqrt{3}$x$\sqrt{3}$ H_3 and T_4 structures;[27] our numbers are 1.12 and 1.61.

Only T2 predicts that all adatom structures are stable as they should be; however, the relative energies are strongly underestimated. With BH, DOD, and T3 all adatom structures are unstable. PTHT predicts that only the H_3 structures are stable. For SW, only the $\sqrt{3}$x$\sqrt{3}$ H_3 surface is stable. With the exception of DOD, all potentials incorrectly favor close packing of adatoms.

According to the DFT calculations,[91,93] in both the T_4 and H_3 structures the three upper atoms surrounding the adatoms relax laterally inward. In the T_4 structures, the adatom is bonded to the three upper atoms and to the second-layer atom directly below; the bond lengths are about the same for both types of neighbors. It is 2.47 and 2.49 Å in the 2x2[91] and $\sqrt{3}$x$\sqrt{3}$[93] structures, respectively; the bond angles are about 92° and 56°. In the H_3 structures, only the three upper atoms are first neighbors of the adatom; for the $\sqrt{3}$x$\sqrt{3}$ structure the bond length is 2.55 Å and the bond angle is 93°.[93] The inward relaxation of the surface atoms in the T_4 structures is predicted by all potentials while in the H_3 structures, only BH, SW, T2, and T3 predict such relaxation. BH and, in particular, SW overestimate significantly the separation between the adatoms and their neighbors in the T_4 structures. For T2, the atomic displacements in the structures are in reasonable agreement with those obtained in the DFT calculations. In general, for all potentials, the structural parameters of the T_4

structures are qualitatively in better agreement with the DFT results than those of the H_3 structures. Consequently, because the surface stress is strongly influenced by the atomic displacements it is qualitatively better described in the T_4 structures. These adatom structures are under a strong tensile stress which is consistent with the inward relaxation of the three surface atoms surrounding the adatom. The greater this relaxation, the larger the positive surface stress.

For all potentials with the exception of T2, the energy gain resulting from the reduction of the dangling bond density is not enough to overcome the strain energy caused primarily by the very small bond angles (Fig. 4). For T2, because the angular function is more flexible and the bond bending forces are small (see Sec. 2), it is able to give a better description of the energetics of these surfaces than the other potentials. Even for those cases where the relative energy of the various adatom structures is positive, the adsorption energy is negative as it should be.

6.2.4 Si(111) $\sqrt{3}$x$\sqrt{3}$ - Vacancy Model

For the vacancy model of the $\sqrt{3}$x$\sqrt{3}$ surface, all potentials correctly predict that this structure is not stable. The vacancy formation energy (with respect to the ideal 1x1 surface) is however significantly overestimated by all potentials with the exception of SW which predicts a value of 0.24 eV/vacancy compared to the DFT value of 0.42 eV/vacancy. The DFT calculation predicts a moderate inward relaxation (toward the vacancy) of the second-layer atoms and a large compression of the first interlayer spacing. No value for the surface stress is available. With BH and SW, the structure is under a strong tensile stress reflecting the large inward relaxation of the second layer atoms which results in a large bond stretching. On the other hand, PTHT, DOD, and T3 give a compressive stress which also reflects the outward relaxation in this case. Finally, consistent with the lack of relaxation, T2 gives a very small stress. For a complete discussion of the vacancy structure the reader is directed to Refs. 37 and 148.

6.2.5 Si(111) (2n+1)x(2n+1)

The DAS model for the Si(111) (2n+1)x(2n+1) surface is well known and the reader is directed to Refs. 141, 144, and 145 for a complete description of the

structure. This surface contains several structural units which are the dimers along the domain walls, T_4 adatoms with a local 2x2 symmetry, stacking faults, and corner holes (an extended surface vacancy). The surface energy is the result of a balance between the individual contributions of these units and possibly the interactions between them. This surface is obviously the most stringent test for the potentials.

Our results, presented in Table VIII, show that only T2 predicts that the 7x7 DAS structure is stable with respect to the ideal 1x1 surface. Furthermore, it is the ground state of the (111) surface at least compared with the structures considered so far. However, as before, the energy is underestimated. Considering the fact that it is also only T2 which predicts that the 2x2 T_4 structure is stable, we conclude that the adatoms play a major role in determining the energy of the 7x7 surface. To confirm this, we have also calculated the energy of the same surface but without the adatoms, the so-called DS model. [85] The relative energy of this structure is indeed very small; it is negative in the case of PTHT, DOD, and T2. The energy difference between the DAS and DS structures should give the contribution of the adatoms to the total energy of the DAS structure if their interaction with the other structural units is negligible. This energy difference is 1.47, 1.25, 1.92, 1.69, -0.48, and 2.39 eV/adatom for PTHT, BH, SW, DOD, T2, and T3, respectively. Except for PTHT, this energy compares fairly well with the contribution of the adatoms to the 2x2 T_4 structure (0.93, 1.38, 2.05, 1.82, -0.31, 2.54 eV/adatom) indicating perhaps that the adatoms do not interact (or very little) with the other features on the surface. Note that the energies of the faulted and unfaulted 2x2 T_4 structures are nearly identical. [85,91] In the representation provided by these potentials, the adatoms play an important role in determining the energy of the 7x7 surface. All potentials predict that the 7x7 DAS surface is under tension in agreement with the estimate of Vanderbilt. [85] Considering the small value of the stress of the corresponding DS structure, most of the tension is caused by the adatoms. Our results obtained with SW and T2 for the 7x7 DAS surface agree with those of Ref. 27 where the structural parameters of the optimized structures were also reported. The investigation of the vibrational spectrum of this surface showed that, despite their limitations, these two potentials are able to accurately describe the z-polarized adatom vibrations. [27]

It has been shown that the different (2n+1)x(2n+1) structures are very close in energy. [16,85,140] For example, Qian and Chadi, using a tight-binding method,

found that the 7x7 DAS structure is only 0.008 eV/1x1 cell lower in energy than the 5x5 DAS structure. [140] It is natural to question whether T2 is able to predict such a trend and also whether the 7x7 reconstruction is indeed the lowest-energy structure. Thus, we have performed calculations for (2n+1)x(2n+1) DAS and DS structures with n = 1 - 4. The relative energy and surface stress for these structures are plotted as a function of n in Fig. 11. T2 does predict the low energy difference between the different structures, about 0.1 eV/ 1x1 cell; however, contrary to what was previuosly thought, [27] the 3x3 DAS structure is the ground state of the Si(111) surface in contradiction with the experimental observation. The energies of the DS and DAS structures appear to increase linearly with n for $n \geq 2$. The surface stress, on the other hand, decreases with increasing n.

We can estimate the energies of the different surface structural units in the DS structures by using Vanderbilt's model based on non-interacting surface units. [16,144,146] In this model, the surface energy per 1x1 cell of the (2n+1)x(2n+1) DS structures, $\Delta\gamma_{DS}$, relative to that of the relaxed 1x1 surface, p, is given by, [16]

$$\Delta\gamma_{DS} = \frac{n(2n+1)\Delta f + 2n\Delta w + \Delta c}{(2n+1)^2} \qquad (8)$$

where $\Delta f = \gamma^{relaxed}_{1x1\text{-}faulted} - p$ is the 1x1 surface faulting energy; $\Delta w = \frac{3}{2}d - p$ is the relative domain wall creation energy (d is the dimer energy); $\Delta c = c - p$ is the relative corner hole energy. Using p = 0.702 eV/1x1 cell, a least square fit yields Δw = -0.45 eV (d = 0.17 eV), Δc = 0.37 eV (c = 1.07 eV), and Δf = 0.0009 eV. The fact that the model gives a vanishingly small value for Δf (recall that T2 predicts that Δf = 0) proves that the assumption of non-interacting structural units is essentially valid. In Ref. 146, the parameters used in (8) (obtained from a combination of DFT and Keating potential calculations) are Δw = -0.66 eV (d = 0.53 eV), Δc = 1.26 eV (c = 2.71 eV), and Δf = 0.06 eV. T2 appears to give too small a value for the relative corner hole energy.

Similar calculations using the other five potentials show that the surface energies and stresses of the (2n+1)x(2n+1) DS and DAS structures decrease with increasing n. For n = 4, the surface energies are already almost equal to

those of the relaxed 1x1 and the 2x2 T_4 structures, respectively. The energies of the DS structures were also fitted to (8) using p and Δf as given in (6.2.1) and Table VIII. When Δf was left as a free parameter, the resulting faulting energy was in poor agreement with the actual value. The results obtained with PTHT, BH, SW, DOD, and T3 are: Δw = -0.32, 0.68, 0.34, 0.62, and 0.68 eV and Δc = 3.15, 0.82, 0.97, 1.63, and 1.27 eV. Like T2, PTHT gives a negative relative domain wall creation energy. The other four potentials give a relative corner hole energy that is in fair agreement with the result of Ref. 146. These potentials favor large n because Δc is too high (PTHT) or Δw is positive (BH, SW, DOD, and T3).

6.3 Si(110)

Like the (100) and (111) surfaces, the Si(110) surface exhibits various reconstructions; [151] however, in contrast to the former, very little interest has been paid to this surface. Only the ideal and relaxed 1x1 surfaces are considered here. No attempt was made to look for reconstructed structures. The bulk terminated surface is formed by chains of atoms running parallel to $[1\bar{1}0]$ (chosen as the x direction; the y direction is taken as $[00\bar{1}]$). Like the (111) surface, this surface has one dangling bond per surface atom pointing in the $\langle 111 \rangle$ direction. Adjacent atoms along a surface chain have dangling bond alternating in directions (pointing in the [111] and $[11\bar{1}]$ directions) and making an angle of $\pm$ 35.3° with the surface normal (they are all normal to the surface on the (111) surface). This surface is modeled with a slab containing 15 layers of 24 atoms each. The bottom four layers were held fixed. The surface energy and stresses are presented in Table IX.

Note that, because they have the same number of dangling bonds per surface atom, the ideal (111) and (110) 1x1 surfaces have also the same surface energy when it is expressed in eV/1x1 cell. For the long-range potentials, PTHT and BH, γ is slightly different because atoms in the top layers have slightly different number of neighbors on the two surfaces. The same is true for the surface stress along $[1\bar{1}0]$. Recall that the surface stress of the (111) 1x1 surface is isotropic. As for the (100) and (111) surfaces, PTHT, DOD, and T3 give a larger relaxation energy (which correlates more or less with the first interlayer contraction) than BH and T2. As discussed earlier, there is no relaxation with

SW. Unlike the (100) and (111) surfaces where relaxation involved only normal displacements of atoms (mainly of the top two layers), the surface atoms of the (110) surface (and to lesser extent those of the second layer), relax radially inward along the ⟨111⟩ direction. That is, in addition to the inward displacement normal to the surface, there is a smaller displacement in the plane of the surface and perpendicular to the chains. This lateral displacement results in a shortening and an increase of the bond lengths and angles in the chains, respectively (2.29 Å and 114° for PTHT and T3, 2.31 Å and 112° for BH and T2, and 2.26 Å and 116° for DOD). The trend in surface energy for the 1x1 surfaces is $\gamma(111) < \gamma(110) < \gamma(100)$ with all potentials. The same trend is obtained for the relaxation energy, $\Delta\gamma$, with PTHT, DOD, and T3. With BH and T2 it is $\Delta\gamma(100) < \Delta\gamma(110) < \Delta\gamma(111)$ and $\Delta\gamma(110) < \Delta\gamma(111) < \Delta\gamma(100)$, respectively. Note that for this comparison these energies were first converted to the true units of surface energy, e.g., $eV/Å^2$.

7 OTHER POTENTIALS

Recently, several new potentials have been proposed. These models, either inspired by earlier attempts or using new schemes, were intended to overcome the limitations of their precursors, i.e., the potentials considered in this work. It is thus worthwhile to review some of them. We should also mention a new class of total-energy functionals for semiconductors which are based on an approximate quantum-mechanical analysis. [32,152]

7.1 Kaxiras and Pandey

Kaxiras and Pandey [21] constructed a potential, very similar in form to BH, in order to specifically simulate processes in the bulk diamond lattice. The potential was fitted to the entire energy surface of atomic exchange obtained from an accurate DFT calculation. [115] It correctly predicts the static properties of the perfect diamond lattice and reproduces the energy of the concerted exchange path to better than 0.1 eV. However, the energies of bulk point defects in their unrelaxed configuration appear to be too low. For the high-coordination crystal phases, the results are qualitatively similar to those obtained with BH. The potential was not tested for surfaces and clusters but it is expected that its predictions would also be similar to those of BH. Because the potential describes

a large range of local distortions from the perfect tetrahedral configuration very well, it should be useful in simulations of systems such as amorphous structures where the coordination remains predominantly four-fold.

7.2 Mistriotis, Flytzanis, and Farantos

Mistriotis, Flytzanis, and Farantos [19] modified the SW potential in order to correctly describe clusters with more than six atoms. The angular dependence of the three-body term was modified and they added a four-body term. The modified potential has not been extensively characterized. It has not been tested for surfaces. It predicts T_m to be about 2050 K and the high-density crystal phases are not well described.

7.3 Khor and Das Sarma

Following Abell [153] and then Tersoff, [8,12] Khor and Das Sarma [14] developed a universal interatomic potential for tetrahedrally bonded semiconductors. The original potential for silicon gives an excellent description of the static properties of cubic diamond as well as the other high-density crystal phases. The potential had to be somewhat extended to correctly treat surfaces. [15] The bond-bending term was modified to deal with the larger angular distortions from the tetrahedral angle encountered on the various (111) surfaces. Also, because the bonds of a given atom can be of a different nature, they had to fix, in an ad-hoc manner, the value of the effective coordination number and assumed that the character of the bonds remains unchanged in the course of the simulation. The modified potential gave a good description of the various (111) surfaces including the adatom structures and the Pandey π-bonded chain model for the 2x1 surface. The results for the (100) surface are similar to those predicted by T2. Yet another modification of the bond-bending term had to be made in order to successfully model the (111) (2n+1)x(2n+1) DAS surfaces. [16] It is not clear how these modifications affect properties previously determined. The original potential and its two modifications are in fact three different potentials just as are T2 and T3. Finally, these potentials have not been tested for bulk point defects and small clusters.

7.4 Bolding and Andersen.

Bolding and Andersen [20] developed a potential which is a generalization of the Tersoff potential. The attractive term is expressed as a sum of σ- and π-bonding terms. Interactions up to five-body are included in the potential. The functional form is complicated and there are over 30 parameters in this potential. The fitting data base was very large and included the static properties of the cubic diamond phase, the fact that the first pressure-induced phase transformation from cubic diamond is to the β-tin phase, and finally the energies and geometries of global and local minima for clusters of 2 - 10 atoms. For small clusters, this potential generates a surface that has most of the minima (global and local) predicted by the ab initio calculations. However, there is not, in general, a one-to-one correspondence between the minima. The ground state structures are predicted to have energies that are in excellent agreement with those of quantum-mechanical calculations. The static properties of cubic diamond silicon are well described but the potential fails to predict the negative Cauchy discrepancy. For bulk point defects, only the vacancy is predicted to have a formation energy in good agreement with the DFT results. The energies of the interstitials, in particular the tetrahedral interstitial, are underestimated. The (111) 2x1 surface is well described. For the adatom structures of the (111) surface, this potential predicts results that are qualitatively similar to those obtained with T2. However, unlike T2, it predicts that the (111) 7x7 DAS surface is unstable with respect to the ideal (111) surface. Finally, for the (100) surface, the predictions are similar to those of T3.

7.5 Thermodynamic Interatomic Force Field

Chelikowsky, Phillips, Kamal, and Strauss [18] developed an interatomic potential similar in form to Tersoff's. The motivation for constructing this potential was to study the metallic to covalent transition which occurs in clusters when the cluster size reaches a critical size. The angular dependence of the bond-bending forces was intended to describe such a transition. The potential describes the perfect diamond structure and the high-density polymorphs of silicon very well. To model clusters, it was found necessary to introduce a so-called dangling-bond vector which describes the transfer of bond strength from a dangling bond to back bonds. The energies of Si_n clusters with $n<10$ are, however, still underestimated. Also, the ground state structures are in general not correct , e.g., for n = 3, 4 and 6. The authors predict that their potential

should be more useful for $n \geq 10$. The potential was not tested for bulk point defects and for surfaces.

7.6 Modified Embedded Atom Method

Baskes, Nelson, and Wright [11] proposed a new potential based on the embedded atom method. [4] The modification consisted of the introduction of an angular dependence in the host electron density. This was necessary for an adequate description of the bond- bending forces in the diamond cubic structure. This potential was extensively tested by its authors. It gives a fit to the energies of the high-density polymorphs comparable to some of the potentials considered here. It describes exactly the static properties of cubic diamond. In particular, unlike most other potentials it does predict the negative Cauchy discrepency. It also provides a fair description of bulk point defects (in particular the vacancy); however, it gives a high value for the energy of the intrinsic stacking fault in silicon. In general, surfaces are poorly described. The potential predicts an outward relaxation of the surface layer for all surfaces. The description of small clusters is in general poor.

8 DISCUSSIONS AND CONCLUSIONS

We have performed extensive calculations on clusters, bulk phases, and surfaces using the PTHT, BH, SW, DOD, T2, and T3 potentials for silicon. In general, no potential is able to model properly all the equilibrium structures and energies of small Si_n ($n = 2 - 6$) clusters. More importantly, they all predict many spurious minima on the potential energy surface of these microclusters. The potentials do, however, predict, like the ab initio calculations, that the structures derived from crystal fragments are not energetically favorable even though the potentials were built from crystal data. T2 gives the best overall description of these small clusters.

In general with the exception of the Dodson potential, the potentials do not accurately describe the energies of the high-pressure bulk phases. A two-dimensional structure with hexagonal symmetry is predicted by PTHT as the most stable structure instead of the diamond cubic phase. Only T3 correctly predicts the first pressure-induced phase transformation from diamond cubic to the β-tin phase with transition pressure and volumes which are in excellent

agreement with experiment. SW, T3, and to a lesser extent DOD, describe the elastic properties well. T2 also does a good job with the exception of the vanishingly small value of C_{44}. BH gives the best description of the phonon frequencies even though it overestimates the elastic constants.

T3, SW, DOD, T2, and BH, in that order, give a fair overall description of the structures and energetics of intrinsic defects. They should be useful in studies of extended defects. PTHT underestimates strongly the energies of these defects. T2 and BH also underestimates significantly the energies of the split vacancy and of the tetrahedral interstitial, respectively. Only BH and SW correctly predict the apparently now more accepted inward relaxation of the neighbouring atoms surrounding the vacancy. SW yields a migration energy for the vacancy which is in excellent agreement with experiment.

BH, SW, T3, and to a lesser extent T2 should also be useful in large-scale simulations involving the (100) surface because their predictions of its energetics and structures are in good agreement with those of the first principles calculations. On the other hand, none of the potentials is able to model the various reconstructions of the (111) surface. None of them model the 2x1 reconstruction of the (111) surface correctly because of their inability to model π-bonding which stabilizes this reconstruction. PTHT predicts that this reconstruction is stable with respect to the ideal 1x1 surface but with a relative energy that is too small. T2 predicts that the ground state for the (111) surface is the 3x3 DAS structure instead of the 7x7 DAS structure as previously thought. As for the microclusters, T2 gives perhaps the best overall description of the (111) surface.

BH and SW tend to overestimate bond lengths. In fact these two potentials, along with T3, have, in general, similar predictions. and so do the PTHT and Dodson potentials. These similar behaviors correlate with similar angular variations of the three-body potentials, in form not necessarily in strength. The difference in strength is somewhat compensated for by an opposite difference in strength of the two-body potentials. T2 is dissimilar precisely because its three-body potential differs markedly from that of the others. That these similarities exist is quite remarkable since, except for SW and BH, these potentials are quite different in schemes, functional forms, and range of interactions. This attests to the importance of the bond-bending forces in these low-order potentials. Besides the fact that they do not model π-bonding, the main reason behind their inability to be more transferable is an inadequate description of the angular forces. They

either favor only small angular distortions around the tetrahedral angle (BH and SW, around 127^{o} for T3) or configurations where bond angles are much larger than the tetrahedral angle (PTHT and DOD). They all penalize, with the exception of T2, angles smaller than about 90^{o} when in fact many structures in silicon involve such small angles, e.g., microclusters and some (111) surfaces. The angular function of T2 is more flexible. It appears that each type of environment, i.e., bulk, clusters, and perhaps surfaces, needs its own angular function. The combined function should then be oscillatory in nature and would be determined by an appropriate selection of relevant structures and energies in the fitting database. Bolding and Andersen did just that.[20] The resulting potential models clusters rather well and gives a description of bulk properties comparable to that of some of the potentials considered here. However, it still failed to model properly (111) surfaces with the exception of the 2x1 reconstruction despite the fact interactions up to five-body were included in the potential. This leads us to believe that it is perhaps not possible to construct a totally global or transferrable potential.

In conclusion, none of the potentials considered in this work appear to be superior to the others. Each has its strengths and limitations. None is totally transferrable. Despite their shortcomings, we do believe that, some of these potentials will be useful in large scale simulations of materials-related problems as they can give insights into phenomena which are otherwise intractable to investigate either experimentally or with first principles methods.

ACKNOWLEDGEMENTS

This work was supported by NSF-DMR-83-16982-A1 through the Center of Materials Research at Stanford, by a grant from NASA, Ames Research Center to Eloret Institute (NCC2-297) and by the Semiconductor Research Corporation under contract no. SRC 90-SP-101.

REFERENCES

1 J. Ihm, Rep. Prog. Phys. 51, 105 (1988); and references therein.

2 R. Car and M. Parrinello, Phys. Rev. Lett. 55, 2471 (1985).

3 C.R.A. Catlow and W.C. Mackrodt, Computer Simulation of Solids, (Springer, New York, 1982).

4 M.S. Daw and M.I. Baskes, Phys. Rev. B 29, 6443 (1984); S.M. Foiles, M.I. Baskes, and M.S. Daw, Phys. Rev. B 33, 7983 (1986).

5 E.M. Pearson, T. Takai, T. Halicioglu, and W.A. Tiller, J. Crystal Growth 70, 33 (1984).

6 F.H. Stillinger and T.A. Weber, Phys. Rev. B 31, 5262 (1985).

7 R. Biswas and D.R. Hamann, Phys. Rev. Lett. 55, 2001 (1985).

8 J. Tersoff, Phys. Rev. Lett. 56, 632 (1986).

9 B.W. Dodson, Phys. Rev. B 35, 2795 (1987).

10 R. Biswas and D.R. Hamann, Phys. Rev. B 36, 6434 (1987).

11 M.I. Baskes, Phys. Rev. Lett. 59, 2666 (1987); M.I. Baskes, J.S. Nelson, and A.F. Wright, Phys. Rev. B 40, 6085 (1989).

12 J. Tersoff, Phys. Rev. B 37, 6991 (1988).

13 J. Tersoff, Phys. Rev. B 38, 9902 (1988).

14 K.E. Khor and S. Das Sarma, Phys. Rev. B 38, 3318 (1988).

15 K.E. Khor and S. Das Sarma, Phys. Rev. B 39, 1188 (1989).

16 K.E. Khor and S. Das Sarma, Phys. Rev. B 40, 1319 (1989).

17 G. Ackland, Phys. Rev. B 40, 10351 (1989).

18 J.R. Chelikowsky, J.C. Phillips, M. Kamal, and M. Strauss, Phys. Rev. Lett. 62, 292 (1989).

19 A.D. Mistriotis, N. Flytzanis, and S.C. Farantos, Phys. Rev. B 39, 1212 (1989).

20 Barry. C. Bolding and Hans C. Andersen, Phys. Rev. B 41, 10568 (1990).

21 Efthimios Kaxiras and K.C. Pandey, Phys. Rev. B 38, 12736 (1988).

22 D.W. Brenner and B.J. Garrison, Phys. Rev. B 34, 1304 (1986).

23 W.A. Harrison, Electronic Structure and the Properties of Solids (Dover, New York, 1989).

24 R. Osgood III and W.A. Harrison, Phys. Rev. B 43, 14255 (1991).

25 A.M. Stoneham, V.T.B. Torres, P.M. Masri, and H.R. Schober, Phil. Mag. A, 58, 93 (1988).

26 K.E. Khor and S. Das Sarma, Phys. Rev. B 36, 7733 (1987).

27 X.P. Li, G. Chen, P.B. Allen, and J.Q. Broughton, Phys. Rev. B 38, 3331 (1988).

28 T. Halicioglu, H.O. Pamok, and S. Erkoc, Phys. Stat. Sol. B 149, 81 (1988).

29 N.C. Bartelt, E.D. Williams, R.J. Phaneuf, Y. Yang, and S. Das Sarmas, J. Vac. Sci. Techn. A 7, 1898 (1989).

30 T. Takai, PhD thesis, Stanford University, Stanford, California (1984).

31 A.E. Carlsson, in Advances in Research and Applications, edited by H. Ehrenreich and D. Turnbull, Solid State Physics, vol. 43 (Academic, New York 1990).

32 A.E. Carlsson, P.A. Fedders, and Charles W. Myles, Phys. Rev. B 41, 1247 (1990).

33 T. Takai, T. Halicioglu, and W.A. Tiller, Scripta Met. 19, 709 (1985).

34 E.M. Pearson, PhD thesis, Stanford University, Stanford, California (1985).

35 E.M. Pearson, T. Halicioglu, and W.A. Tiller, Surf. Sci. 184, 401 (1987).

36 T. Takai, T. Halicioglu, and W.A. Tiller, Surf. Sci. 164, 341 (1985).

37 H. Balamane, T. Halicioglu, and W.A. Tiller, Phys. Rev. B 40, 9999 (1989).

38 T. Takai, T. Halicioglu, and W.A. Tiller, Surf. Sci. 164, 327 (1985).

39 H. Balamane, T. Halicioglu, and W.A. Tiller, J. Crystal Growth 85, 16 (1987).

40 D.K. Choi, T. Takai, S. Erkoc, T. Halicioglu, and W.A. Tiller, J. Crystal Growth 85, 9 (1987).

41 D.K. Choi, S.M. Koch, T. Takai, T. Halicioglu, and W.A. Tiller, J. Vac. Sci. Techn. B 6, 1140 (1988).

42 W.A. Tiller, J. Vac. Sci. Techn. A7, 1353 (1989).

43 R. Biswas, G.S. Grest, and C.M. Soukoulis, Phys. Rev. B 36, 7437 (1987).

44 R. Biswas, G.S. Grest, and C.M. Soukoulis, Phys. Rev. B 38, 8154 (1988).

45 I. Kwon, R. biswas, G.S. Grest, and C.M. Soukoulis, Phys. Rev. B 41, 3678 (1990).

46 E. Blaisten-Baroja and D. Levesque, Phys. Rev. B 34, 3910 (1986).

47 B.P. Feuston, R.K. Kalia, and P. Vashishta, Phys. Rev. B 35, 6222 (1987).

48 E.R. Cowley, Phys. Rev. Lett. 60, 2379 (1988).

49 Mark D. Kluge, John R. Ray, and Aneesur Rahman, J. Chem. Phys. 85, 4028 (1986).

50 I.P. Batra, F.F. Abraham, and S. Ciraci, Phys. Rev. B 35, 9552 (1987).

51 Marcia H. Grabow, George H. Gilmer, and Aloysius F. Bakker, Mat. Res. Soc. Symp. Proc., Vol 141 (Materials Research Society, 1989) p. 349.

52 W.D. Luedtke and U. Landman, Phys. Rev. B 37, 4656 (1988).

53 W.D. Luedtke and U. Landman, Phys. Rev. B 40 1164 (1989).

54 P.C. Kelires and J. Tersoff, Phys. Rev. Lett. 61, 562 (1988).

55 Mark D. Kluge, JohnR. Ray, Aneesur Rahman, Phys. Rev. B 36, 4234 (1987).

56 K.E. Khor and S. Das Sarma, Chem. Phys. Lett. 134, 43 (1987).

57 S. Das Sarma, S.M. Paik, K.E. Khor, and A. Kobayashi, J. Vac. Sci. Techn. B 5, 1179 (1987).

58 J.H. Wilson, J.D. Todd, and A.P. Sutton J. Phys.: Condens. Matter 2, 10259 (1990).

59 T.A. Weber, Mat. Res. Soc. Symp. Proc., Vol 63 (Materials Research Society, 1985) p. 163.

60 Tze Wing Poon, Sidney Yip, Paul S. Ho, and Farid F. Abraham, Phys. Rev. Lett. 65, 2161 (1990).

61 Z.Q. Wang and D. Stroud, Phys. Rev. B 38, 1384 (1988).

62 U. Landeman, W.D. Luedtke, R.N. Barnett, C.L. Cleveland, M.W. Ribarsky, E.A.S. Ramesh, H. Baumgart, A. Martinez, and B. Khan, Phys. Rev. Lett. 56, 155 (1986).

63 F.F. Abraham, and J.Q. Broughton, Phys. Rev. Lett. 56, 734 (1986).

64 B.W. Dodson, Phys. Rev. B 33, 7361 (1986).

65 M. Schneider, I.K. Schuller, and A. Rahman, Phys. Rev. B 36, 1340 (1987).

66 Zhenyu Zhang and Horia Metin, Surf. Sci. 245, 353 (1991).

67 U. Landeman, W.D. Luedtke, M.W. Ribarsky, R.N. Barnett, and C.L. Cleveland, Phys. Rev. B 37, 4637 (1988).

68 W.D. Luedtke, U. Landeman, M.W. Ribarsky, R.N. Barnett, and C.L. Cleveland, Phys. Rev. B 37, 4647 (1988).

69 E.T. Gawlinski and J.D. Gunton, Phys. Rev. B 36, 4774 (1987).

70 W.D. Luedtke and U. Landman, to be published in Phys. Rev. B 40, 11733 (1989).

71 K. Ding and H.C. Andersen, Phys. Rev. B 34, 6987 (1986).

72 F. H. Stillinger, T.A. Weber, and R.A. Laviolette, J. Chem. Phys. 85, 6460 (1986); F. H. Stillinger and T.A. Weber, J. Phys. Chem., 91, 4899 (1987).

73 F.H. Stillinger and T.A. Weber, J. Chem. Phys. 88, 5123 (1988).

74 F.H. Stillinger and T.A. Weber, Phys. Rev. Lett. 62, 2144 (1989).

75 S.M. Foiles, Phys. Rev. B 32, 3409 (1985).

76 Donald W. Brenner, Phys. Rev. Lett. 63, 1022 (1989).

77 B.W. Dodson, Phys. Rev. B 36, 1068 (1987).

78 M.I. Heggie, Phil. Mag. Lett. 58, 75 (1988).

79 M. Kitabatake, P. Fons, and J.E. Greene, J. Vac. Sci. Techn. A 8, 3726 (1990).

80 J. Tersoff, Phys. Rev. Lett. 61, 2879 (1988).

81 J. Tersoff, Phys. Rev. B 39, 5566 (1989).

82 P.C. Kelires and J. Tersoff, Phys. Rev. Lett. 63, 1164 (1989).

83 Steve Langhoff, private communication.

84 D.C. Wallace, Thermodynamics of Crystals (John Wiley & Sons, New York, 1972).

85 D. Vanderbilt, Phys. Rev. Lett. 59, 1456 (1987); and references therein.

86 M.C. Payne, N. Roberts, R.J. Needs, M. Needels, and J.D. Joannopoulos, Surf. Sci. 211/212, 1 (1989); and references therein.

87 F.F. Abraham, Advances in Phys. 35, 1 (1986).

88 K. Raghavachari, J. Chem. Phys. 84, 5672 (1986); and references therein.

89 M.T. Yin and M.L. Cohen, Phys. Rev. B. 26, 5668 (1982); and references therein.

90 Inder P. Batra, Phys. Rev. B. 41, 5048 (1990).

91 R.D. Meade and D. Vanderbilt, Phys. Rev. B. 40, 3905 (1989).

92 D. Vanderbilt, private communication.

93 J.E. Northrup, Phys. Rev. Lett. 57, 154 (1986); in Proceedings of the Eighteenth International Conference on the Physics of Semiconductors, edited by O. Engstrom (World Scientific, Singapore, 1987).

94 R. Car, P.J. Kelly, A. Oshiyama, and S.T. Pantelides, Phys. Rev. Lett. 52, 1814 (1984) and 54, 360 (1985); G.A. Baraff and M. Schluter Phys. Rev. B

30, 3460 (1984); Y. Bar-Yam and J.D. Joannopoulos Phys. Rev. B 30, 1844 (1984).

95 A. Antonelli and J. Bernholc, Phys. Rev. B 40, 10643 (1989).

96 P.J. Kelly, R. Car, and S.T. Pantelides, in Defects in Semiconductors, edited by H.J. von Bardeleben, Materials Science Forum 10-12 (Trans. Tech. Publications, Aedermannsdorf, Swizterland, 1986) p. 115; and references therein.

97 K.P. Huber and G. Herzberg, "Constants of Diatomic Molecules", (Van Nostrand, New York, 1979).

98 D. Tomanek and M.A. Schluter, Phys. Rev. Lett. 56, 1055 (1986).

99 See references 89, 101-103,107,108, and references therein.

100 S.J. Duclos, Y.K. Vohra, and A.L. Ruoff, Phys. Rev. Lett. 58, 775 (1987).

101 M.T. Yin, Phys. Rev. B. 30, 1773 (1984).

102 M.T. Yin and M.L. Cohen, Phys. Rev. B. 29, 6996 (1984).

103 R.J. Needs and R.M. Martin, Phys. Rev. B. 30, 5390 (1984).

104 A.M. Stoneham and J.H. Harding, Ann. Rev. Phys. Chem. 37, 53 (1986); and references therein.

105 S. Erkoc, T. Halicioglu, and W.A. Tiller, J. Non-Cryst. Solids 94, 28 (1987).

106 I.L.F. ray and D.J.H. Cockayne, Proc. R. Soc. London A 325, 543 (1971); H. Foll and C.B. Carter, Phil. Mag. A 40, 497 (1979).

107 R. Biswas, R.M. Martin, R.J. Needs and O.H. Nielsen, Phys. Rev. B. 30, 3210 (1984).

108 K.J. Chang and M.L. Cohen, Phys. Rev. B. 30, 5376 (1984); 31, 7819 (1985); and references therein.

109 G. Simmons and H. Wang "Single Crystal Elastic Constants and Calculated Aggregate Properties: A Handbook" (MIT Press, Cambridge, Mass., 1971)

110 O.N. Nielsen and R.M. Martin, Phys. Rev. B 32, 3792 (1985).

111 G. Dolling, Inelastic Scattering of Neutrons in Solids and Liquids, Vol. II (IAEA: Vienna, 1963) p. 37.

112 H. D'Amour, W. Denner, Heinz Schulz, and Manuel Cardona, J. Appl. Cryst. 15, 154 (1982).

113 E.O. Kane, Phys. Rev. B. 31, 7865 (1985); and references therein.

114 J.H. Rose, J.R. Smith, F. Guinea, and J. Ferrante, Phys. Rev. B 29, 2963 (1984); and references therein.

115 K.C. Pandey, Phys. Rev. Lett. 57, 2287 (1986).

116 C.Z. Wang, C.T. Chan, and K.M. Ho, Phys. Rev. Lett. 66, 189 (1991).

117 J.A. Barker and D.Henderson, Rev. Mod. Phys. 48, 587 (1976); J.P.Hansen and L.Verlet, Phys. Rev. 184, 151 (1969).

118 D. Haneman, Rep. Prog. Phys. 50, 1045 (1987); Adv. Phys. 31, 165 (1982); and references therein.

119 R.M. Tromp, R.G. Smeenk, F.W. Saris, and D.J. Chadi, Surf. Sci. 133, 137 (1983); and references therein.

120 R.J. Hamers, R.M. Tromp, and J.E. Demuth, Phys. Rev. B. 34, 5343 (1986).

121 J.E. Northrup, Phys. Rev. Lett. 54, 815 (1985).

122 R.M. Tromp, R.J. Hamers, and J.E. Demuth, Phys. Rev. Lett. 55, 1303 (1985).

123 M.T. Yin and M.L. Cohen, Phys. Rev. B. 24, 2303 (1981).

124 K.C. Pandey, in Proceedings of the Seventeenth International Conference on the Physics of Semiconductors, San Francisco, CA, 1984, Eds. D.J. Chadi and W.A. Harrison (Springer, New York, 1985).

125 N. Roberts and R.J. Needs, Surf. Sci. 236, 112 (1990).

126 S. Ihara, S.L. Ho, T. Uda, and M. Hirao, Phys. Rev. Lett. 65, 1909 (1990).

127 This value was obtained by using the relative energy of the 2x1 surface of -0.93 eV/1x1 cell obtained by Batra at 7.5 Ry (Ref. 90) and adding the

energy (with respect to the 2x1 surface) of 0.035 eV/1x1 cell reported in Ref. 125.

128 D.J. Chadi, Phys. Rev. Lett. 43, 43 (1979).

129 J. Nogami, S. Park, and C.F. Quate, Appl. Phys. Lett. 53, 2086 (1988).

130 K. Kato, T. Ide, T. Nishimori, and T. Ichinokawa, Surf. Sci. 207, 177 (1988); K. Müller, E. Land, L. Hammer, W. Grim, P. Heilman, and K. Heinz, in Determination of Surface Structure by LEED, edited by P.M. Marcus and F. Jona (Plenum, New York, 1984), p.483.

131 J.A. Martin, D.E. Savage, W. Moritz, and M.G. Lagally, Phys. Rev. Lett. 56, 1936 (1986); and references therein.

132 F. Ancilotto, W. Ancheoni, A. Selloni, R. Car, and M. Parrinello, Phys. Rev. Lett. 65, 3148 (1990); and references therein.

133 G.B. Adams and Otto F. Sankey, Phys. Rev. Lett. 67, 867 (1991).

134 D. Haneman and A.A. Chernov, Surf. Sci. 215, 135 (1989); and references therein.

135 J.E. Northrup and M.L. Cohen, J. Vac. Sci. Techn. 21, 333 (1982).

136 K.C. Pandey, Phys. Rev. Lett. 47, 1913 (1981).

137 J.E. Northrup and M.L. Cohen, Phys. Rev. Lett. 49, 1349 (1982).

138 O.H. Nielsen, R.M. Martin, D.J. Chadi, and K. Kunc J. Vac. Sci. Techn. B 1, 714 (1983).

139 D. Haneman, Phys. Rev. B 42, 8982 (1990); and references therein.

140 Guo-Xin Qian and D.J. Chadi, Phys. Rev. B. 35, 1288 (1987).

141 K. Takayanagi, Y. Tanishiro, M. Takahashi, and S. Takahashi, J. Vac. Sci. Techn. A 3, 1502 (1985).

142 S.Y. Tong, H. Huang, C.M. Wei, W.E. Packard, F.K. Men, G. Glander, and M.B. Webb, J. Vac. Sci. Techn. A 6, 615 (1988).

143 I.K. Robinson, J. Vac. Sci. Techn. A 6, 1966 (1988).

144 Guo-Xin Qian and D.J. Chadi, J. Vac. Sci. Techn. B 4, 1079 (1986).

145 R.S. Becker, J.A. Golovchenko, G.S. Higashi, and B.S. Swartzentruber, Phys. Rev. Lett. 57, 1020 (1986).

146 D. Vanderbilt, Phys. Rev. B 36, 6209 (1987); and references therein.

147 W.C. Fan, A. Igniatiev, H. Huang, and S.Y. Tong, Phys. Rev. Lett. 62, 1516 (1989).

148 C.T. Chan and K.M. Ho, Phys. Rev. Lett. 64, 491 (1990).

149 The surface energy of the ideal (111) 1x1 surface was not reported in Refs. 85 and 91. The value of 1.56 eV/1x1 cell was obtained by using the reported surface energy of 1.39 eV/1x1 obtained at 12 Ry for the relaxed surface and assuming a relaxation energy of 0.17 eV/1x1 cell as calculated at 6 Ry by Northrup (Ref. 91).

150 J.J. Gilman, J. Appl. Phys. 31, 2208 (1960).

151 E.G. Keim, H. Wormeester, and A. van Silfhout, J. Vac. Sci. Techn. A 8, 2747 (1990); and references therein.

152 W.A. Harrison, Phys. Rev. B 41, 6008 (1990).

153 G.C. Abell, Phys. Rev. B 31, 6184 (1984).

TABLE I. Parameters for the potentials. The units are such that energy and length are in eV and Å, respectively. θ_0 is in degrees.

	PTHT	BH	SW	DOD	T2	T3
R_c	7.3	5.0	3.77118	3.2	3.2	3.0
μ		0.312058	2.0951	0.4	0.4	0.3
σ		3.9527357				
A_1	50928.2584	142.2922	189.360881	1614.6	3264.7	1830.8
A_2	697.005028	107.0338	16.31972277	155.08	95.373	471.18
λ_1	12	0.5200836	4	2.7793	3.2394	2.4799
λ_2	6	0.4206931	0	1.3969	1.3258	1.7322
Z or Z_1	2949.47219	26.0598	48.61499998			
Z_2		1.3441478				
α or α_1		0.3034373	1.2	4	1.3258	1.7322
α_2		0.3191903				
n				0.6207	22.956	0.78734
β				0.13420598	0.33675	1.0999×10^{-6}
η				0.8543	2.80755739	105.2851343
δ				3.9588	2.0417	16.218
θ_0		109.471221	109.471221		90	126.745381

TABLE II. Equilibrium properties of Si_2 and Si_3. r_e and r (Å) are the bond lengths, D_e and E_B (eV) are the binding energies, ω_o (cm^{-1}) is the vibrational frequency, and θ (degrees) is the bond angle. Values in parenthesis correspond to a mechanically stable configuration lying higher in energy. In the second column, the experimental values are for Si_2 (Ref. 97) and KR corresponds to the ab initio results for Si_3 (Ref. 88).

	Experiment/KR	PTHT	BH	SW	DOD	T2	T3
				Si_2			
D_e	3.24	2.38	2.49	2.32	3.61	2.62	2.67
r_e	2.246	2.295	2.233	2.352	2.192	2.313	2.295
ω_o	510.98	794	463	462	521	467	471
				Si_3			
E_B	7.7	5.29	5.39	4.74	7.04	7.87	5.33
	(~ 7.6)	(5.23)		(4.63)	(6.05)		(4.81)
θ	77.8	180	60	60	180	60	126.75
	(60)	(60)		(109.47)	(60)		(60)
r	2.17	2.27	2.42	2.56	2.20	2.31	2.30
	(2.26)	(2.39)		(2.35)	(2.40)		(2.50)

TABLE III. Properties of Si_4 - Si_6. The first three most stable structures are given in the order of decreasing binding energy. For each structure, the first entry is the binding energy E_B (eV), the others are bond lengths (Å), and angle (degrees). KR corresponds to the ab initio results of Ref. 88. The asterisk indicates that this structure is known to be not a minima on the quantum-mechanical surface. The different structures along with the corresponding structural parameters are illustrated in Fig. 5. The acronyms are: tetrahedron (T_d); edge-capped rhombus (ECR); corner-capped triangle and rhombus (CCT,CCR); pentagonal, square, and distorted pentagonal pyramid (PP,SP,DPP); flat and elongated trigonal bipyramid (FTB,ETB); orthorhombic bipyramid (OB); edge-and face-capped trigonal bipyramid (ECTB,FCTB). For the linear structures, the numbering of atoms is from one end to the other.

	KR	PTHT	BH	SW	DOD	T2	T3
Si_4	rhombus 12.85 r_{12} = 2.30 r_{13} = 2.40	rhombus 8.48 2.37 2.59	square* 8.93 2.34	square* 8.69 2.39	linear* 10.48 r_{12} = 2.20 r_{23} = 2.21	T_d 15.71 2.31	square* 8.64 2.38
	D_{2d} 11.53	square* 8.44 2.34	T_d 8.25 2.56	T_d 7.13 2.72	square* 9.73 2.33	rhombus 13.10 2.31 2.31	chain 8.00 r = 2.30 θ = 126.75
	T_d 9.71 2.46	CCT* 8.33 r_{12} = 2.26 r_{13} = 2.36	CCT* 7.38 r_{12} = 2.30 r_{13} = 2.45	chain 6.95 2.35 109.5	rhombus 9.53 2.40 2.55	square* 10.49 2.31	linear* 7.41 2.32 2.34
Si_5	FTB 16.70 r_{12} = 3.26 r_{14} = 2.34 r_{45} = 2.78	ECR 12.04 r_{12} = 2.34 r_{14} = 2.56 r_{24} = 2.37	pentagon 12.08 2.28	pentagon 11.57 2.35	pentagon 14.25 2.28	ETB 20.40 2.37 2.35 3.84	pentagon 12.44 2.32
	ETB 15.62 2.48 2.40 3.86	pentagon 11.88 2.31	ESP* 11.90 2.47 2.64	FTB 11.46 3.25 2.50 3.29	linear 13.91 r_{12} = 2.20 r_{23} = 2.21	FSP 20.13 2.34 2.32	CCR 11.27 2.38 3.50 2.30
	FSP 13.90 r_{12} = 2.48 r_{15} = 2.36	CCR 11.65 r_{12} = 2.34 r_{24} = 2.59 r_{15} = 2.26	FTB 11.82 3.02 2.46 3.48	ESP* 11.01 2.46 2.85	CCR 13.09 2.36 3.15 2.21	FTB 16.98 3.50 2.34 2.34	FTB 10.95 3.36 2.45 3.00
Si_6	ECTB 21.91	hexagon 15.31 2.28	wedge 15.81 r_{12} = 2.53 r_{14} = 2.40	wedge 15.15 2.60 2.40	hexagon 18.48 2.25	octahedron 26.52 2.37	hexagon 15.79 2.30
	hexagonal chair 15.98	PP 14.72 r_{12} = 2.41 r_{16} = 2.50	PP 15.71 2.41 2.63	DPP 15.12	linear 17.34 r_{12} = 2.20 r_{23} = 2.21 r_{34} = 2.21	FCTB* 26.22	asymmetric 14.83 3.19 3.26
		asymmetric 14.63 r_{12} = 2.47 r_{34} = 2.63	asymmetric 15.46 3.26 3.63	asymmetric 15.07 3.34 3.36	PP 16.40 2.43 2.53	OB 23.95	wedge 14.33 2.54 2.43

TABLE IV. Equilibrium properties of optimized bulk silicon structures. $\Delta E = E_C - E_C(\text{diamond})$ and E_C is the cohesive energy (eV/atom). a (Å) and B (Mbar) are the lattice parameter and bulk modulus, respectively. x is the internal parameter of the BC-8 structure; it is given in units of a. In the DFT column, the results for BC-8 and graphite are from Refs. 101 and 102, respectively, the values of B for simple hexagonal and β-tin are from Ref. 103, and the remaining data are from Ref. 89. The experimental values of E_C and a for diamond are -4.63 eV and 5.429 Å, respectively.

		DFT	PTHT	BH	SW	DOD	T2	T3
Diamond	E_C	-4.67	-4.63	-4.6045	-4.63	-4.63	-4.6304	-4.6297
	a	5.451	5.435	5.432	5.431	5.432	5.431	5.432
Hexagonal Diamond	ΔE	0.016	0.0012	0.012	0.0	0.0	0.0	0.0
	a	3.858	3.846	3.841	3.840	3.841	3.841	3.841
	c/a	1.633	1.630	1.639	1.633	1.633	1.633	1.633
BC-8	ΔE	0.13	0.311	0.238	0.201	0.207	0.026	0.245
	a	6.67	6.682	6.730	6.591	6.588	6.579	6.644
	x	0.1003	0.1034	0.1015	0.1016	0.1054	0.1018	0.1008
	B	0.96	2.73	2.05	0.85	0.96	1.10	1.03
β-tin	ΔE	0.266	0.576	0.218	0.213	0.350	0.455	0.327
	a	4.822	5.243	5.113	4.969	4.978	4.987	4.905
	c/a	0.552	0.464	0.522	0.561	0.521	0.518	0.524
	B	1.19	2.71	3.08	4.43	2.97	3.40	1.38
Simple Hexagonal	ΔE	0.293	-0.559	0.191	0.403	0.371	0.527	0.469
	a	2.639	2.405	2.762	2.833	2.634	2.613	2.699
	c/a	0.94	2.866	0.956	0.918	0.997	0.985	0.967
	B	1.06		3.11	3.61	1.29	1.40	1.38
Simple Cubic	ΔE	0.348	0.447	0.158	0.293	0.388	0.343	0.318
	a	2.528	2.549	2.609	2.612	2.529	2.501	2.544
BCC	ΔE	0.525	0.916	.312	0.300	0.479	0.644	0.432
	a	3.088	3.165	3.236	3.245	3.153	3.126	3.084
HCP	ΔE	0.552	0.110	0.052	0.321	0.637	0.551	0.761
	a	2.735	4.094	3.973	3.647	2.800	2.730	2.756
	c/a	1.633	0.591	0.685	0.884	1.633	1.633	1.633
FCC	ΔE	0.566	0.950	0.255	0.423	0.628	0.548	0.761
	a	3.885	3.984	4.075	4.147	3.960	3.861	3.897
Graphitic Silicon	ΔE	0.710	0.3177	0.3847	0.6715	0.3625	0.5087	0.5131
	a	3.895	4.123	4.145	4.073	4.094	4.101	4.096
	c/a	2.726	1.215	1.232	1.193	1.193	1.198	1.233
	B	0.50	2.738	2.076	1.667	0.944	1.003	0.984

TABLE V. Elastic and vibrational properties of silicon. The bulk modulus and elastic constants are in Mbar, the phonon frequencies in THz. B' is the pressure derivative of the bulk modulus, C^{o}_{44} is the theoretical value obtained for C_{44} in the absence of internal strain, and ζ is Kleinman's internal strain parameter; their value in column 2 is from Ref. 89, 110, and 112, respectively. The experimental values for B and the elastic constants are from Ref. 109. The phonon frequencies were taken from Ref. 111, 34, 10, 27, and 13 for experiment, PTHT, BH, SW and T2, and T3, respectively.

	Experiment	PTHT	BH	SW	DOD	T2	T3
B	0.99	2.788	1.692	1.083	0.884	0.98	0.98
B'	4.2	7.82	5.66	2.93	4.27	4.58	4.30
C_{11}	1.67	2.969	2.042	1.616	1.206	1.217	1.425
C_{12}	0.65	2.697	1.517	0.816	0.722	0.858	0.754
C_{44}	0.81	0.446	0.451	0.603	0.659	0.103	0.690
C^{o}_{44}	1.11	2.190	1.049	1.172	3.475	0.923	1.188
ζ	0.74	1.03	0.74	0.63	1.06	0.83	0.67
ν_{TA} (X)	4.4	4.5	5.6	6.7		2.7	9
ν_{TO} (X)	13.9	19.3	14.5	15.9		15.3	16
ν_{LOA} (X)	12.3	13.8	12.2	13.1		11.7	12
ν_{LTO} (Γ)	15.3	18.3	16	18.1		16.5	16

TABLE VI. Formation energies (in eV) of intrinsic defects in silicon. The first and second values are for the equilibrium (relaxed) and ideal (unrelaxed) configurations, respectively. The third value is the radial relaxation of nearest-neighbors around the defect (in %); a negative value indicates an inward relaxation towards the defect. I_T, I_H, I_B, and I_S are the tetrahedral, hexagonal, bond-centered, and split interstitials, respectively. The DFT energies and relaxation for the split vacancy and the unrelaxed vacancy formation energy are from Ref. 96; the others are from Ref. 94.

	DFT	PTHT	BH	SW	DOD	T2	T3
Vacancy	3 - 4	0.77	2.12	2.82	2.57	2.81	3.70
	4.5	2.50	3.83	4.63	3.23	2.83	4.10
		38.5	-25.7	-24	14.7	1	10.5
Split Vac.	4.19	2.83	2.30	3.36	4.17	1.40	3.50
	5.01	4.53	4.72	6.00	8.12	4.15	10.5
	-9.5	-15.9	-12.5	-11.8	-14.5	-14.9	-8.8
I_T	5 - 6	0.63	1.56	5.25	3.03	5.03	3.45
		1.91	4.57	12.21	5.00	5.85	6.92
		3.8	8	9	9.1	7.3	10.5
I_H	4 - 5	0.84	2.89	6.95	2.61	3.67	4.61
		5.32	9.31	17.10	5.11	5.39	8.22
		7.4	11.5	14.7	7.3	7.6	10.2
I_B	4 - 5	1.92	2.54	5.99	4.39	2.84	5.86
I_S		1.47	3.30	5.62	3.49	2.32	4.70

TABLE VII. Properties of Si(100) surfaces. γ is the surface energy , $\Delta\gamma$ is the relative energy with respect to the ideal 1x1 surface, and σ is the lateral surface stress tensor. The x and y directions run along the dimer bond and the rows of dimers, respectively. Energies and stresses are given in eV/1x1 cell. Δ is the first interlayer contraction (in %). r_d and r_{bb} (in Å) are the bond lengths of the dimer and the back bond between surface and second-layer atoms. θ_1, θ_2, and θ_3 , are the bond angles as indicated in Fig. 9. The DFT results for the surface energy and the structural parameters of the (2x1) structure are from Ref. 90 and 125, respectively, those for the surface stress are all from Ref. 86, and the remaining data are from Ref. 123 (see text).

	DFT	PTHT	BH	SW	DOD	T2	T3
				ideal 1x1			
γ	2.5	1.805	2.080	2.315	1.779	2.015	2.126
σ_{xx}	2.535	1.176	1.421	0	0	0	0
σ_{yy}	0.855	2.363	1.683	0	0.145	0.625	-0.236
				relaxed 1x1			
$\Delta\gamma$	-0.03	-0.077	-0.027	0	-0.085	-0.004	-0.037
σ_{xx}		-0.427	0.848	0	0.515	0.023	0.076
σ_{yy}		-2.176	0.273	0	-2.775	0.080	-1.693
Δ	-5.1	-7.0	-5.5	0	-10.2	-2.3	-7.2
				2x1			
$\Delta\gamma$	-0.93	-0.690	-0.709	-0.899	-0.714	-1.258	-0.759
σ_{xx}	0.693	-0.808	0.669	1.167	-0.094	0.703	0.367
σ_{yy}	-1.945	-1.731	0.008	-0.051	-1.709	0.190	-1.236
Δ	-24.4	-23.3	-13.3	-8.3	-22.9	-14.6	-15.6
r_d	2.23	2.339	2.403	2.404	2.318	2.328	2.365
r_{bb}	2.29	2.313	2.352	2.367	2.314	2.340	2.336
θ_1	107.8	109.0	106.7	104.8	109.0	106.6	106.7
θ_2	92.9	91.0	94.8	97.9	90.6	94.8	94.7
θ_3	100.8	104.7	103.5	101.0	106.5	103.2	102.8
				c-2x2			
$\Delta\gamma$		-0.839	-0.703	-0.824	-0.720	-1.143	-0.753
σ_{xx}		-1.356	0.898	1.691	0.274	1.517	0.865
σ_{yy}		-1.419	0.851	0.574	-0.866	0.567	-0.344
				Pandey π-bonded defect structure			
$\Delta\gamma$	-0.895 [a]		-0.687	-0.814	-0.045	-1.289	-0.682
σ_{xx}			0.130	0.782	-1.110	1.075	-0.061
σ_{yy}			2.577	3.454	-0.227	1.441	3.075

[a] Ref. 127

TABLE VIII. Properties of Si(111) surfaces. For the ($\sqrt{3}$x$\sqrt{3}$) surface, V stands for the vacancy model. γ is the surface energy , $\Delta\gamma$ the relative energy with respect to the ideal 1x1 surface, and σ is the lateral surface stress tensor. For the 2x1 π-bonded surface, the x and y directions are parallel and perpendicular to the surface chains, respectively. Energies and stresses are given in eV/1x1 cell. Δ is the first interlayer contraction (in %). Unless indicated otherwise, the DFT results are from Ref. 85 and 91 where the stresses were calculated at 8 Ry and the energies at 12 Ry.

		DFT	PTHT	BH	SW	DOD	T2	T3
				ideal (1x1)				
	γ	1.56 [a]	0.831	1.035	1.158	0.806	0.707	1.026
	σ		2.323	0.969	0	0.140	0.625	-0.074
				relaxed (1x1)				
	$\Delta\gamma$	-0.17 [a]	-0.148	-0.012	0	-0.134	-0.005	-0.069
	σ	-0.54	-2.148	0.149	0	-1.664	0.102	-1.241
	Δ	-27.0	-27.6	-8.4	0	-31.7	-6.4	-20.3
				(2x1) π-bonded				
	$\Delta\gamma$	-0.45	-0.150		0.373	0.002	0.091	0.145
	σ_{xx}	1.4	0.252		0.017	-0.770	0.473	-0.663
	σ_{yy}	0.4	0.956		2.236	1.087	1.043	1.711
				(7x7) DAS				
	$\Delta\gamma$	< -0.45	0.240	0.398	0.532	0.390	-0.170	0.625
	σ		2.172	1.297	1.972	1.153	1.614	0.738
				(7x7) DS				
	$\Delta\gamma$		-0.120	0.093	0.062	-0.024	-0.052	0.041
	σ		0.295	0.534	0.980	-0.272	0.559	0.112
				(2x2)				
T_4	$\Delta\gamma$	-0.44	0.085	0.333	0.513	0.320	-0.081	0.566
	σ	1.66	0.949	0.606	1.113	-0.074	1.248	-0.608
H_3	$\Delta\gamma$	-0.33	-0.184	0.191	0.267	0.337	-0.115	0.350
	σ	1.18	-3.606	-0.397	0.234	-3.309	1.391	-0.621
				($\sqrt{3}$x$\sqrt{3}$)				
T_4	$\Delta\gamma$	-0.38	0.206	0.442	0.456	0.447	-0.109	0.774
	σ	1.70	1.449	0.742	2.111	0.371	1.663	-0.388
H_3	$\Delta\gamma$	-0.07 [b]	-0.178	0.260	-0.043	0.478	-0.143	0.482
	σ		-4.143	-0.502	0.724	-3.528	1.705	-0.522
V	$\Delta\gamma$	0.14 [c]	0.44	0.45	0.08	0.43	0.45	0.55
	σ		-2.35	5.26	5.98	-1.32	-0.01	-1.17

[a] Ref. 149
[b] Ref. 93, calculated at 6 Ry.
[c] Ref. 148, calculated at 10.5 Ry.

TABLE IX. Properties of the Si(110) surface. γ is the surface energy , $\Delta\gamma$ the relative energy with respect to the ideal 1x1 surface, and σ is the lateral surface stress tensor. The x and y directions are parallel and perpendicular to the surface chains, respectively. Energies and stresses are given in eV/1x1 cell. Δ is the first interlayer contraction (in %).

	PTHT	BH	SW	DOD	T2	T3
			ideal (1x1)			
γ	0.885	1.043	1.158	0.806	0.707	1.026
σ_{xx}	2.170	0.934	0	0.140	0.625	-0.074
σ_{yy}	1.273	0.714	0	0.385	0.468	0.179
			relaxed (1x1)			
$\Delta\gamma$	-0.080	-0.018	0	-0.068	-0.009	-0.035
σ_{xx}	-1.627	0.063	0	-1.360	0.018	-1.027
σ_{yy}	-1.091	-0.066	0	-0.634	0.063	-0.612
Δ	-5.3	-3.4	0	-6.6	-2.4	-4.3

Figure Captions

Figure 1. Illustration of the geometry of a triplet of atoms used in the definition of the three-body potentials.

Figure 2. Comparison of the two-body potential functions, $V_2(r)$. The open circles correspond to the ab initio calculation of Ref. 83.

Figure 3. Comparison of the angular variation of the three-body potentials, $g(\theta)$, (an isoceles triangle was used for PTHT).

Figure 4. Three-body energy (in eV/atom) versus angle θ for a triplet of atoms forming an isoceles triangle. θ is the apex bond angle between the two equal bond lengths fixed at the equilibrium bond length of the diamond structure of silicon. (see text)

Figure 5. Illustration of the geometry of some structures for Si_5 - Si_6. These are: the rhombus (1), the corner-capped triangle (2), the chain (3), the D_{2d} structure of Ref. 88 (4), the flat trigonal bipyramid (5), the corner- (6) and edge- (7) capped rhombus, the square pyramid (8), the edge- (9) and face- (10) capped trigonal bipyramid, an asymmetric structure (11), a distorted (12) and regular (13) pentagonal pyramid, the orthorhombic bipyramid (14), and the wedge or trigonal prism (15). In the elongated form of the trigonal bipyramid, atoms 1, 2, and 3 are bonded to each other and the apex atoms are widely spaced.

Figure 6. Binding energy per atom versus the number of atoms in the cluster in Si_2 - Si_6. The curve KR corresponds to the ab initio results of Ref. 88.

Figure 7. Comparison of cohesive energy for various bulk silicon structures. For the graphitic and HCP structures, see text.

Figure 8. Comparison of energy versus first-nearest neighbor distance for the cubic diamond structure.

Figure 9. Side view of the Si(100)-2x1 surface showing the symmetric dimer reconstruction. The arrows indicate the atomic displacements (in Å) from the bulk terminated positions. The four values (starting from the top) correspond to DFT(Ref. 125), BH, SW, and T3, respectively. The displacements for T2 are similar to those for T3; those for PTHT and

DOD are somewhat different. The cartesian coordinate system is also shown; the y direction runs into the page and is along $[\bar{1}10]$.

Figure 10. Side view of the Pandey π-bonded defect structure for the Si(100) surface. The cartesian coordinate system is the same as in Fig. 9.

Figure 11. Relative energy with respect to the ideal 1x1 surface and surface stress for the Si(111) (2n+1)x(2n+1) DAS (open circles) and DS(filled circles) structures as a function of n for the T2 potential.

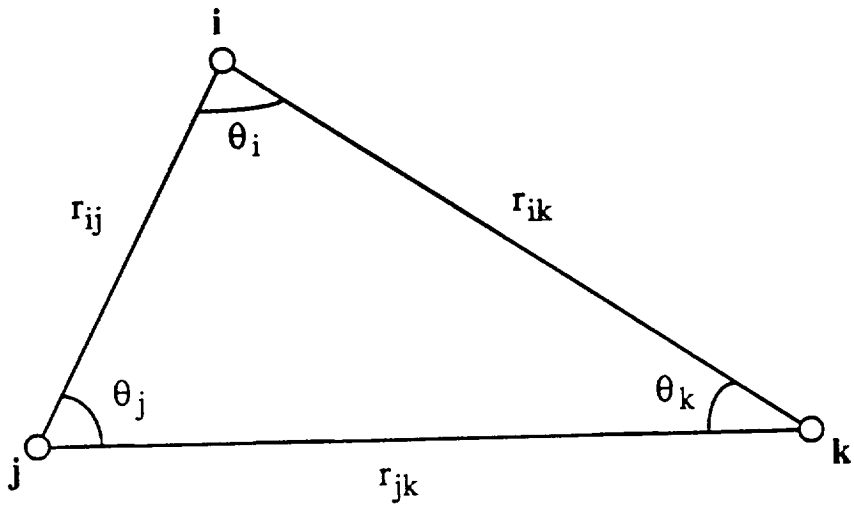

Figure 1

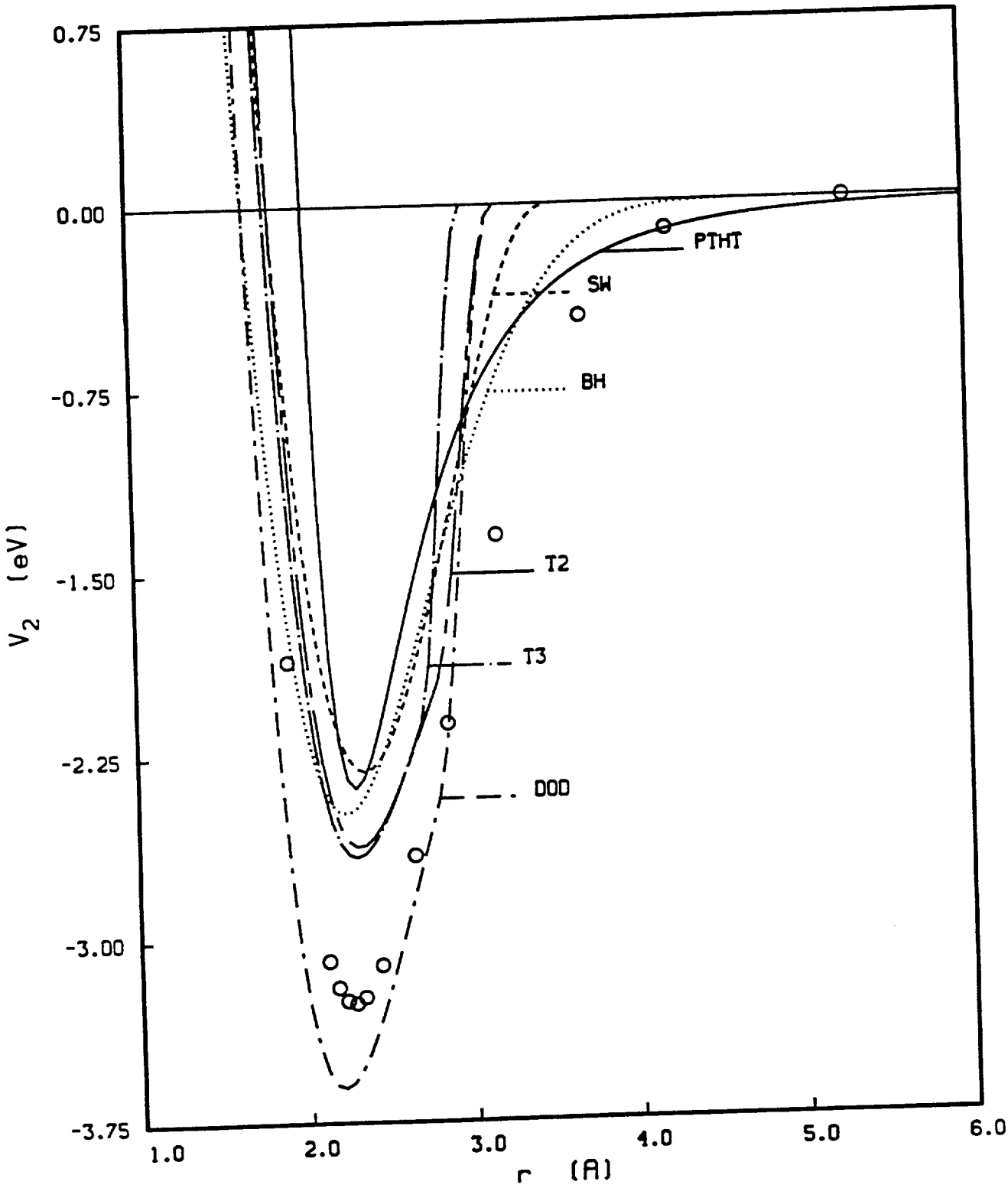
0.75
0.00
-0.75
-1.50
-2.25
-3.00
-3.75
V_2 (eV)
1.0
2.0
3.0
4.0
5.0
6.0
r (A)
PTHT
SW
BH
T2
T3
DOD

Figure 2

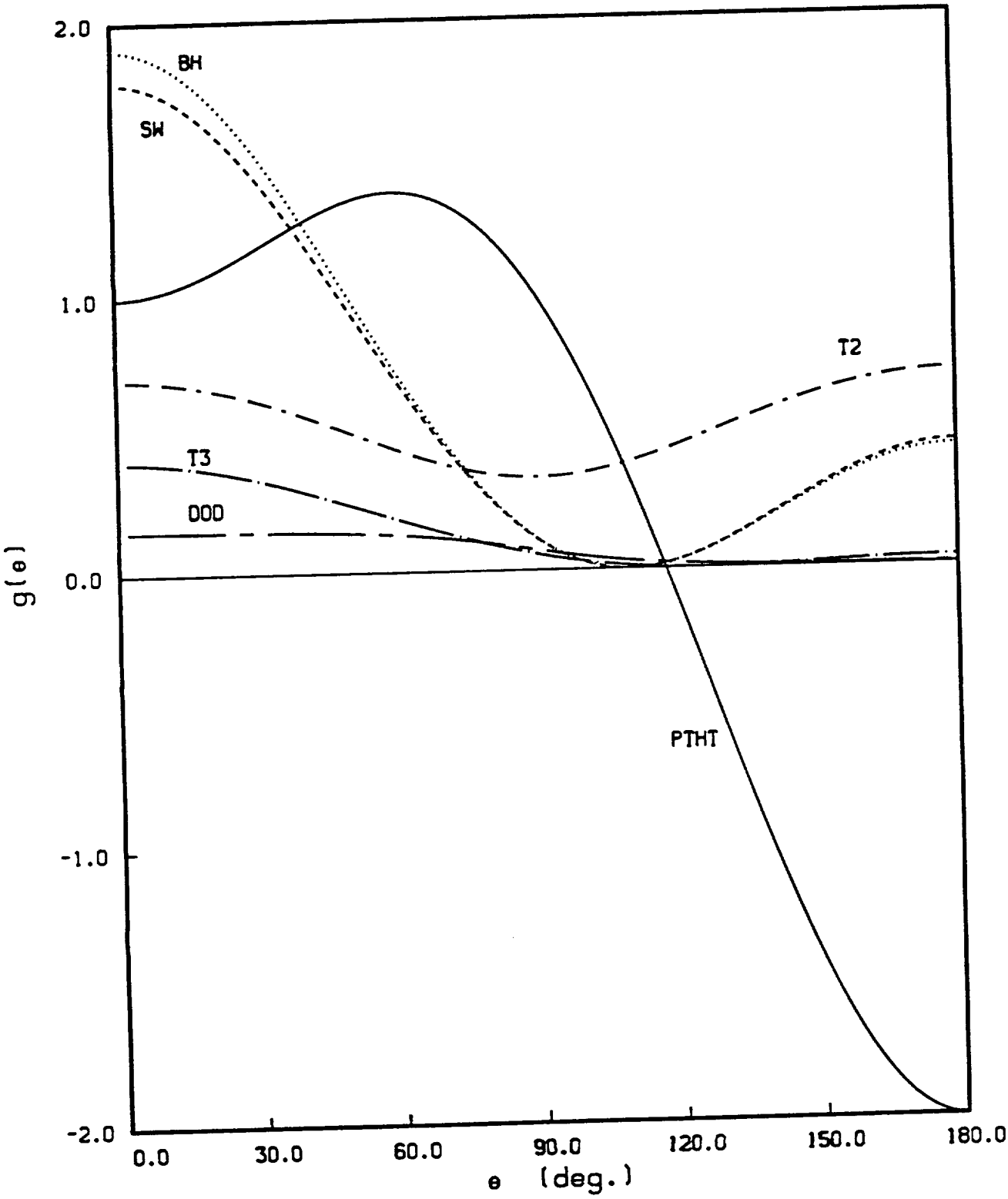
2.0
1.0
0.0
-1.0
-2.0
g(e)
BH
SW
T2
T3
DDD
PTHT
0.0
30.0
60.0
90.0
120.0
150.0
180.0
e (deg.)

Figure 3

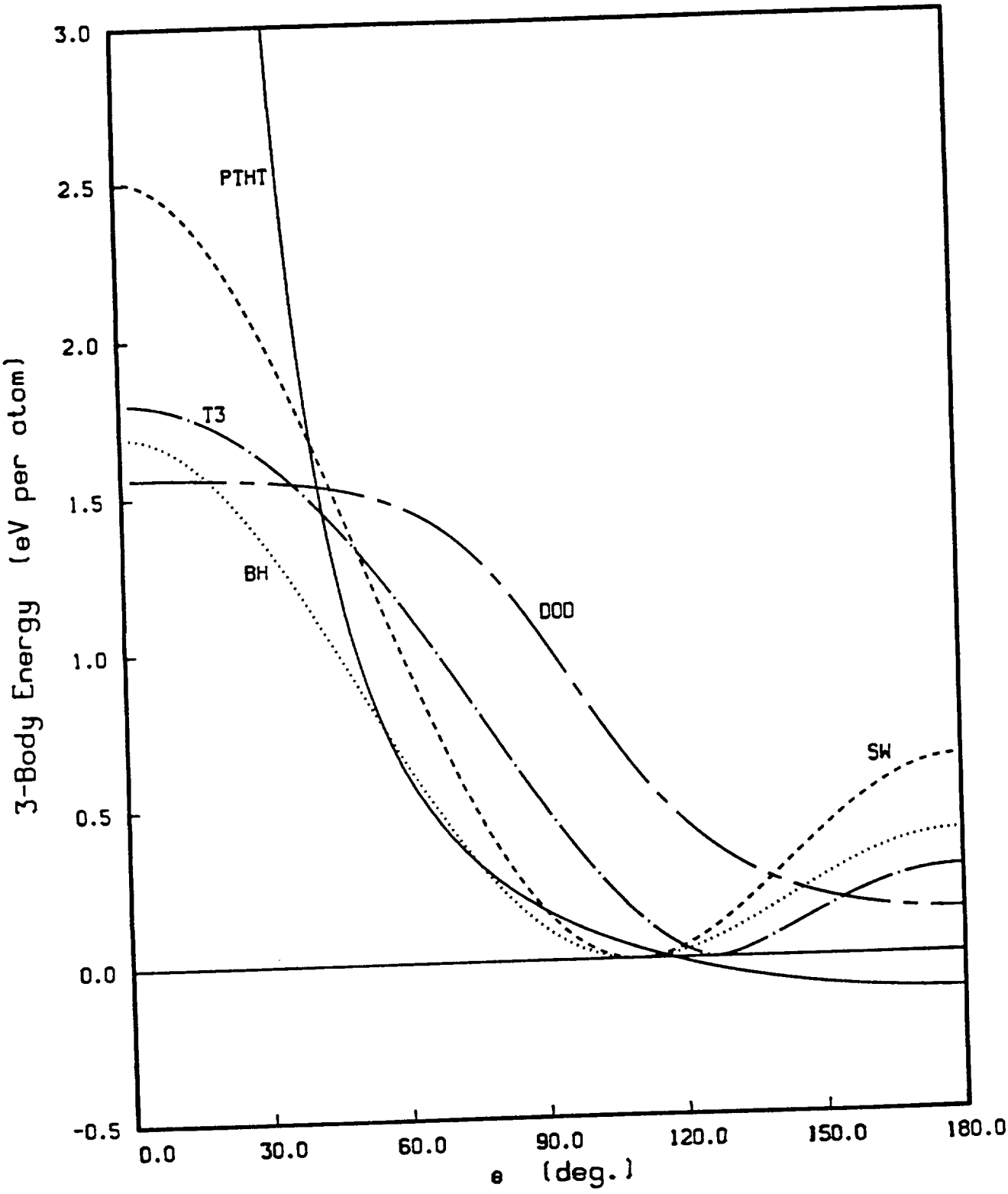
3.0
2.5
2.0
1.5
1.0
0.5
0.0
-0.5
3-Body Energy (eV per atom)
PTHT
T3
BH
DOD
SW
0.0
30.0
60.0
90.0
120.0
150.0
180.0
θ (deg.)

Figure 4

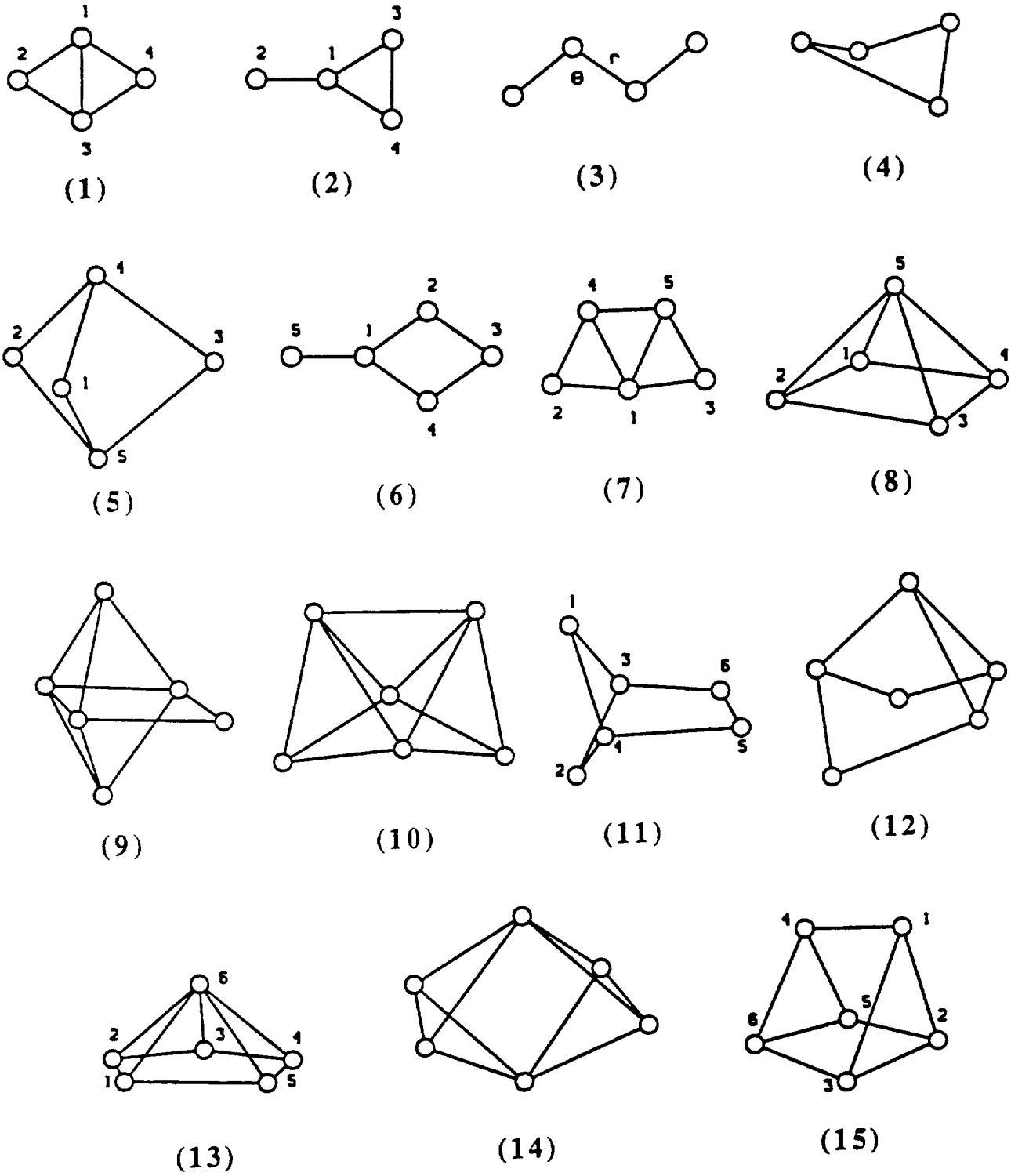

Figure 5

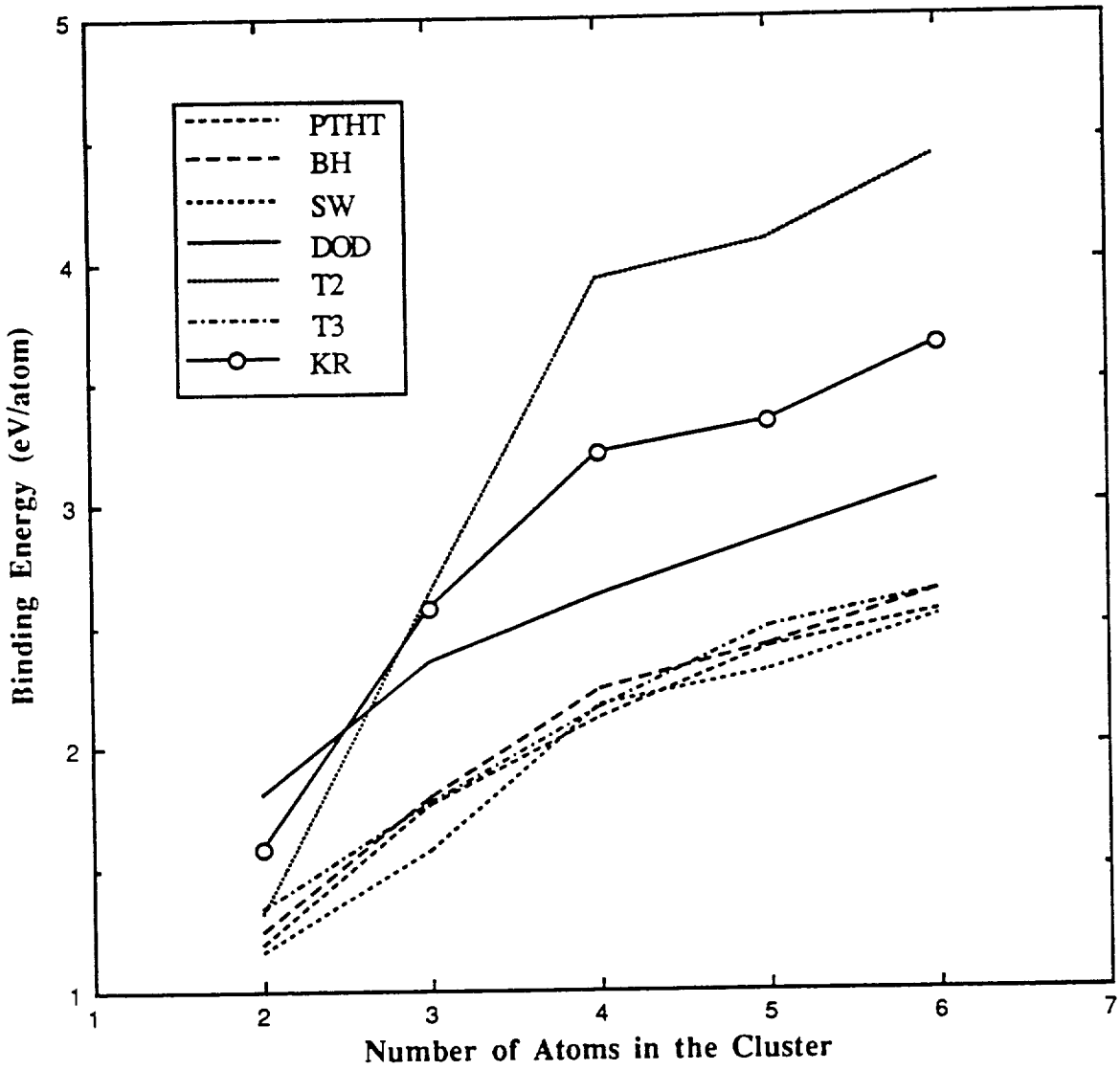
PTHT
BH
SW
DOD
T2
T3
KR
Binding Energy (eV/atom)
Number of Atoms in the Cluster
1
2
3
4
5
6
7

Figure 6

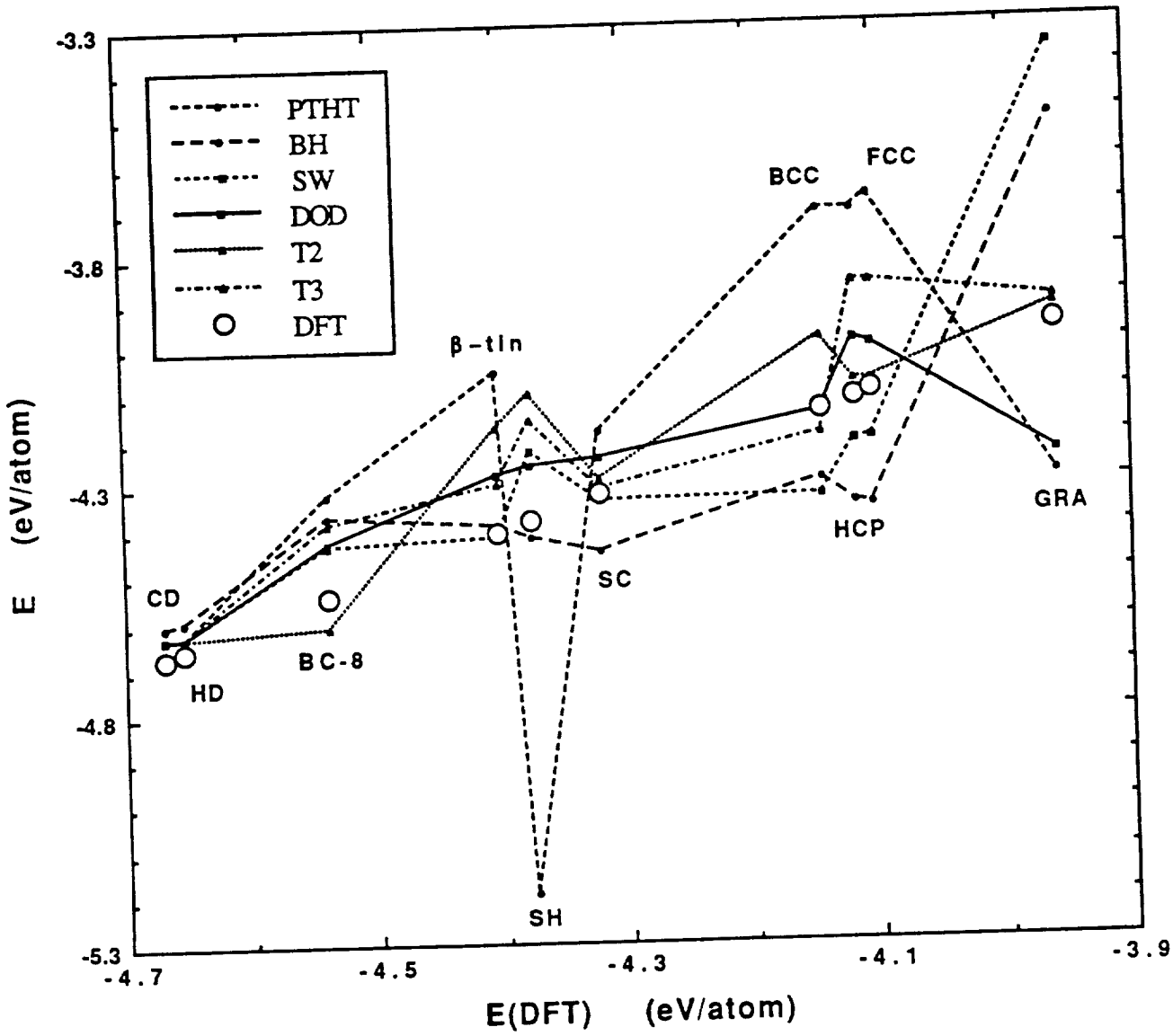
PTHT
BH
SW
DOD
T2
T3
DFT
-3.3
-3.8
-4.3
-4.8
-5.3
E (eV/atom)
-4.7
-4.5
-4.3
-4.1
-3.9
E(DFT) (eV/atom)
β-tin
BCC
FCC
HCP
GRA
SC
SH
CD
HD
BC-8

Figure 7

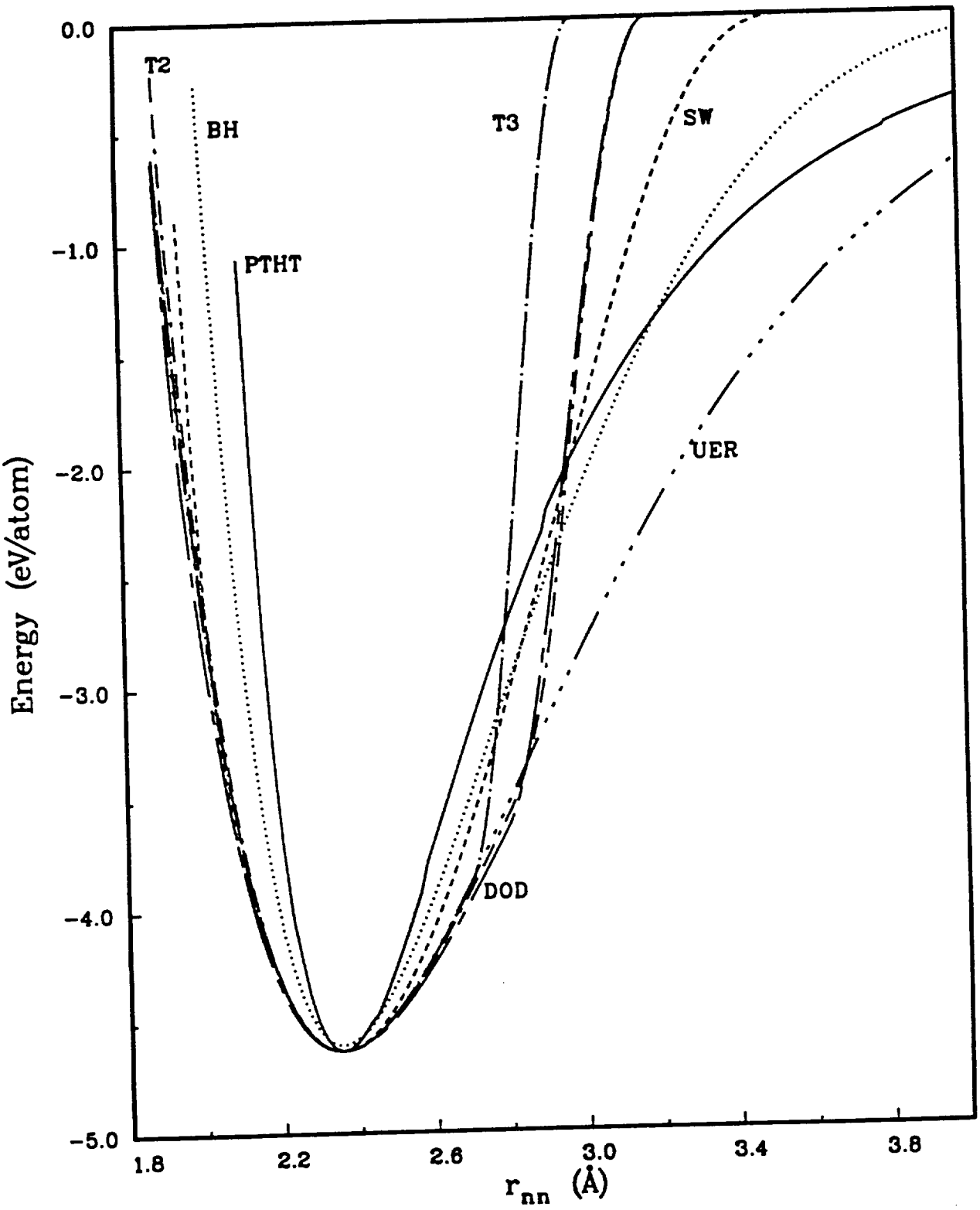
0.0
-1.0
-2.0
-3.0
-4.0
-5.0
Energy (eV/atom)
1.8
2.2
2.6
3.0
3.4
3.8
r_{nn} (Å)
T2
BH
PTHT
T3
SW
UER
DOD

Figure 8

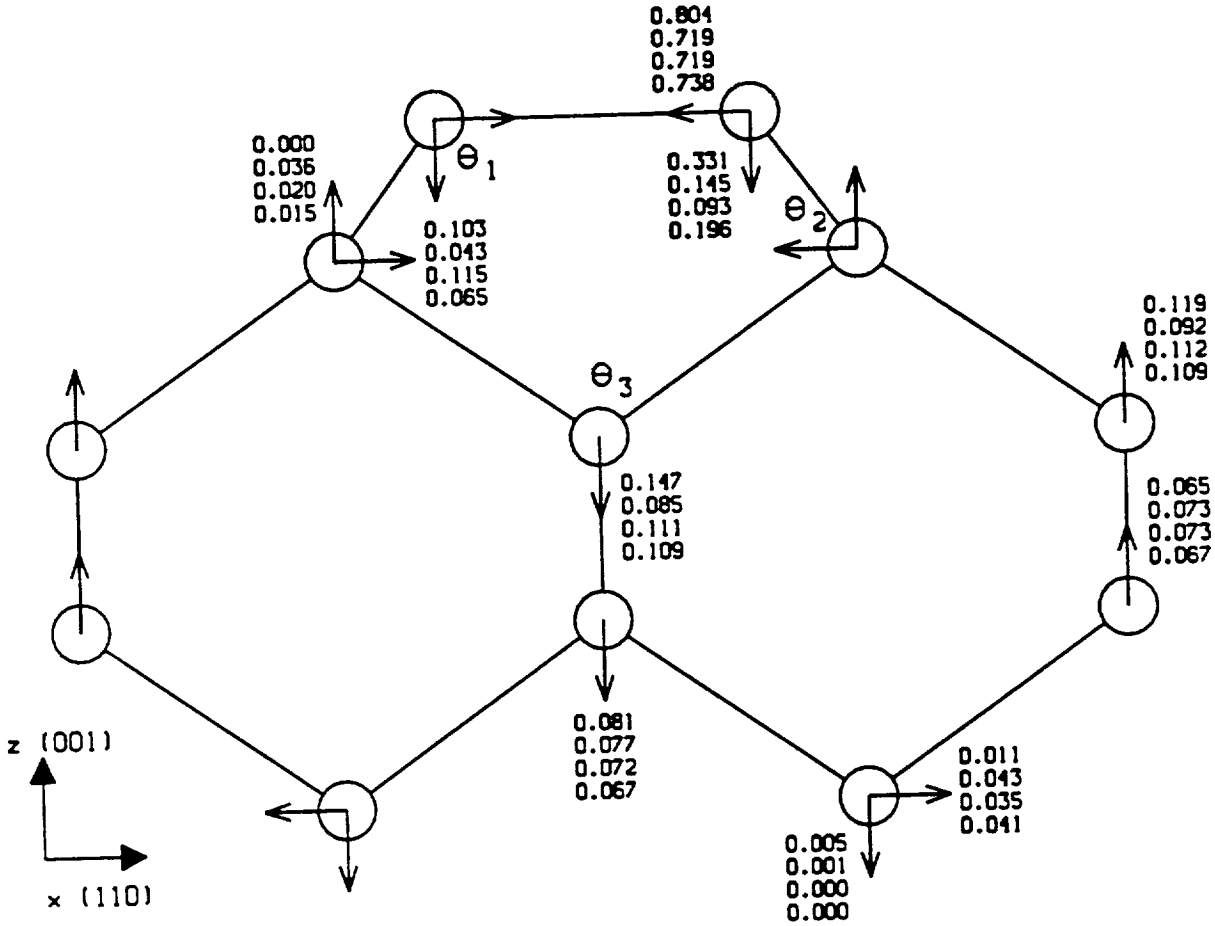
0.804
0.719
0.719
0.738
0.000
0.036
0.020
0.015
θ1
0.331
0.145
0.093
0.196
θ2
0.103
0.043
0.115
0.065
0.119
0.092
0.112
0.109
θ3
0.147
0.085
0.111
0.109
0.065
0.073
0.073
0.067
0.081
0.077
0.072
0.067
0.011
0.043
0.035
0.041
0.005
0.001
0.000
0.000
z (001)
x (110)

Figure 9

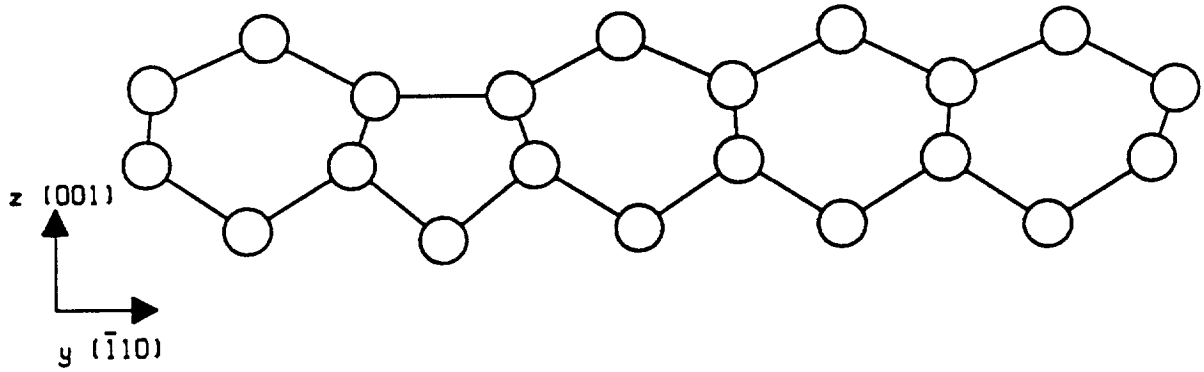

Figure 10

C-2

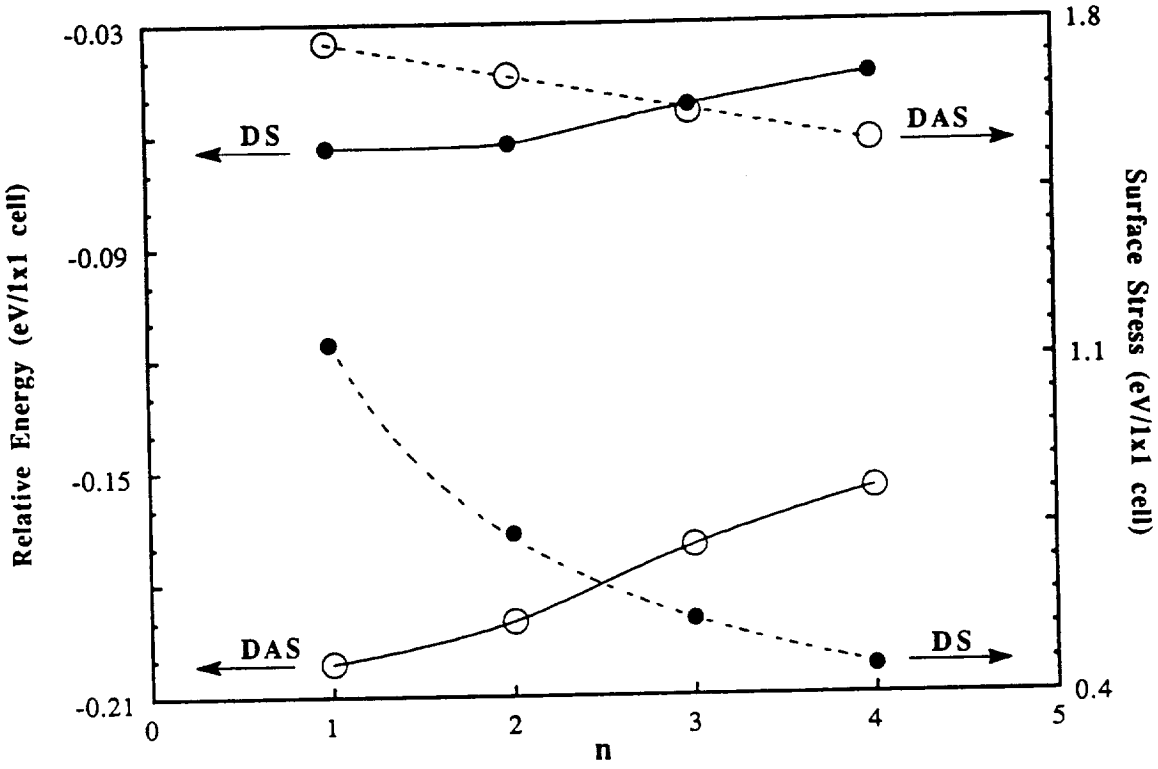
-0.03
-0.09
-0.15
-0.21
Relative Energy (eV/1x1 cell)
DS
DAS
DAS
DS
1.8
1.1
0.4
Surface Stress (eV/1x1 cell)
0
1
2
3
4
5
n

Figure 11